Resolving the origins of secretory products and anthelmintic responses in a human parasitic nematode at single-cell resolution.

Clair R. Henthorn[1], Paul M. Airs[1], Emma Neumann[2], Mostafa Zamanian[1*]
[1] Department of Pathobiological Sciences, University of Wisconsin-Madison, Madison, WI USA
[2] Pathology and Laboratory Medicine, School of Medicine and Public Health, University of Wisconsin-Madison, Madison, WI USA
[*] mzamanian@wisc.edu

Abstract

Nematode excretory-secretory (ES) products are essential for the establishment and maintenance of infections in mammals and are valued as therapeutic and diagnostic targets. While parasite effector proteins contribute to host immune evasion and anthelmintics have been shown to modulate secretory behaviors, little is known about the cellular origins of ES products or the tissue distributions of drug targets. We leveraged single-cell approaches in the human parasite *Brugia malayi* to generate an annotated cell expression atlas of microfilariae. We show that prominent antigens are transcriptionally derived from both secretory and non-secretory cell and tissue types, and anthelmintic targets display distinct expression patterns across neuromuscular and other cell types. While the major classes of anthelmintics do not affect the viability of isolated cells at pharmacological concentrations, we observe cell-specific transcriptional shifts in response to ivermectin. Finally, we introduce a microfilariae cell culture model to enable future functional studies of parasitic nematode cells. We expect these methods to be readily adaptable to other parasitic nematode species and stages.

Introduction

Lymphatic filariasis (LF) is a chronic and debilitating neglected tropical disease caused by the filarial nematodes *Wuchereria bancrofti, Brugia malayi, and Brugia timori.* Infective-stage larvae are transmitted by mosquitoes to the human definitive host, where they develop and molt to adult stages that persist in the lymphatics and produce blood-circulating pre-larval stage microfilariae (mf) (Roberts et al., 2009). LF afflicts an estimated 51 million individuals in tropical and subtropical climates around the world and endangers nearly a billion individuals worldwide (Local Burden of Disease 2019 Neglected Tropical Diseases Collaborators, 2020; World Health Organization, 2018). Chronic cases of LF manifest in elephantiasis, an extreme buildup of lymph resulting in stigmatizing disfiguration and additional socioeconomic challenges (Ton et al., 2015; Weiss, 2008). Mass drug administration in endemic settings with combinations of ivermectin, diethylcarbamazine (DEC), and albendazole is used to disrupt parasite transmission, but this approach is only effective with years of repeated treatment. Additionally, contraindications for antifilarial drugs exist in regions co-endemic for other filarial parasites (Chippaux et al., 1996). With no cure and the growing threat of resistance to anthelmintics (Campbell, 1982; Geary et al., 2011, 2010a; Ismail et al., 1999; Osei-Atweneboana et al., 2011; Wolstenholme et al., 2015), there is a clear need to improve our understanding of basic biological processes that underpin the host-parasite interaction.

The excretory-secretory (ES) products of parasitic nematodes are known to be essential for parasite survival within the host (Harnett, 2014; Hotterbeekx et al., 2021; Lightowlers and Rickard, 1988). Despite the general understanding that the ES system is a conduit for the release of immunomodulatory proteins and extracellular vesicles that promote parasite survival, the biology of the ES system has yet to be investigated in medically important parasitic nematodes. Profiling of secretions (Bennuru et al., 2011; Harischandra et al., 2018; Hewitson et al., 2008; Kaushal et al., 1982; Moreno and Geary, 2008; Zamanian et al., 2015) across the filarial nematode life cycle has helped identify antigens that have been pursued therapeutically and diagnostically (Harnett, 2014; Kalyanasundaram et al., 2020; Maizels et al., 2001; Morris et al., 2013), but the origins of these proteins and the tissue systems that underlie their release at the host-parasite interface are unknown. Recent studies have also implicated secretory processes as a target of existing anthelmintics (Moreno et al., 2021, 2010). Ivermectin causes rapid clearance of mf from host blood at concentrations that do not cause overt fitness effects on cultured parasites (Geary et al., 2010b). This disconnect is reconciled by a model whereby ivermectin unmasks mf from the host immune system by inhibiting protein and vesicle secretion (Rao et al., 1987; Vatta et al., 2014; Zahner et al., 1997). While the ES apparatus is thought to be the primary source of immunogenic proteins in the mf stage, the cells that comprise this structure and control secretion have not been characterized.

Clear morphological descriptions of the filarial ES system are currently restricted to the mf stage, but microscopy studies confirm that this structure is present in L3 and adult parasites (Airs et al., 2022; Landmann et al., 2010; Mutafchiev et al., 2014; Tongu, 1974). Filarial parasites possess tubular ES systems featuring a single large excretory cell connected through a cytoplasmic bridge to an excretory vesicle and pore (Tongu, 1974). In the free-living model nematode *Caenorhabditis elegans*, the ES system is a well-studied and critical os-moregulatory and excretory organ made up of a pore cell, duct cell, excretory/canal cell, and canal-associated neurons (CAN) (Sundaram and Buechner, 2016). However, significant diversification of ES anatomy and function between *C. elegans* and filariae and more generally across nematode clades (A. F. Bird, 1991) demands more species-specific approaches to the study of excretory-secretory systems.

Single-cell transcriptomics has facilitated resolution of cellular processes and functions that are masked in tissue level or bulk transcriptomic approaches. Cell dispersions of free-living nematodes (Zhang et al., 2011) have enabled high dimensional transcriptomic analysis of cell types across developmental stages (Ben-David et al., 2020; Cao et al., 2017; Packer et al., 2019; Taylor et al., 2021; Zhang et al., 2011)1) and provide a pathway to the characterization of essential cells and tissues in related parasites, including those that control secretory behaviors. However, viable cell suspensions have yet to be leveraged to transcriptomically profile human, animal, or plant parasitic nematodes at single-cell resolution. This goal is complicated in many species by life cycle patterns that can limit tissue availability and anatomical variation that can affect access to rare cell types.

Here, we applied single-cell approaches to generate and annotate a cell atlas of gene expression in *Brugia malayi* microfilariae and to map secretory-associated cell types and the distributions of prominent antigens and anthelmintic targets. We evaluated the effects of anthelmintics on parasite cells and the amenability of mf cell suspensions to longer-term culture. These data and methods allowed for novel inferences about the origins of immunogenic molecules, the mechanism of action of existing anthelmintics, and provide an avenue for future functional studies of *B. malayi* cell populations. We expect that many of these tools can be extended to other medically important parasitic nematodes.

Results

Generation of viable single-cell suspensions from *Brugia malayi* microfilariae

We focused our efforts on generating single-cell dispersions from the blood-circulating microfilariae (mf) stage of the human parasitic nematode *B. malayi*. This pre-larval life stage is small (~177-230 µm in length, ~5-7 µm in diameter) but can be isolated from peritoneal fluid of infected jirds in large quantities (millions), potentially facilitating insight into early parasite development and the capture of rare cell types. Using larval dispersion protocols from *C. elegans* as a scaffold, we developed a single-cell dispersion protocol in *B. malayi* mf that accounts for the unique biology of this parasite stage (**Figure 1A**). Microfilariae (mf) suspensions recovered from the jird peritoneal cavity are developmentally asynchronous and include a slew of host cells, tissue debris, embryos, and nonviable mf, all of which contribute to transcriptic contamination. To reduce contamination and enrich for viable mf, peritoneal lavages were filtered using Sephadex PD-10 desalting columns (Galal et al., 1989; Rathaur et al., 1987). This method reliably recovered high yields (60-70%) of highly motile mf which were then used as input into single-cell dispersion reactions (**Figure 1B**).

B. malayi mf are encapsulated within an impermeable eggshell of carbohydrates including chitin (Fuhrman and Piessens, 1985). We treated filtered mf with chitinase to penetrate this sheath and allow downstream dispersion reagents to access the underlying cuticle and worm body. Chitinase treatment (2 mg/mL for 20 min at 37°C) did not cause complete exsheathment, but produced a visible shrinking effect in the tail and head spaces indicating sheath breachment (**Figure 1C**). SDS-DTT treatment was optimized to weaken protective structures (sheath and cuticle) of chitinase-treated worms while preserving cell health. Incubation in diluted SDS-DTT (1:4 in L-15 for 6 min) effectively compromised cuticular structure and inhibited motility without causing parasite death (**Supp. Figure 1**). Recoverable inhibition of motility, as revealed by subsequent wash steps, serves as visual confirmation of the efficient weakening of the cuticle and preservation of the underlying body.

Dispersions of single-cells were then performed using pronase enzymatic digestion (15 mg/mL) and mechanical disruption by continuous pipetting. Progression of the pronase digestion was monitored throughout the treatment (**Figure 1D)**. mf cuticles were visibly compromised after approximately 20 min of digestion, where the midsection of the filarial body plan exhibits protrusions which break and release cells. Progression of the reaction yields a mixed suspension of worm segments, single-cells, and intact mf, and an abundance of single-cells can be seen by 30 min. Continuous mechanical disruption was essential to encourage the breakage of worms and release of single-cells. The majority of undigested worms were removed by centrifugation and filtration resulting in a highly viable single-cell mf suspension for downstream applications.

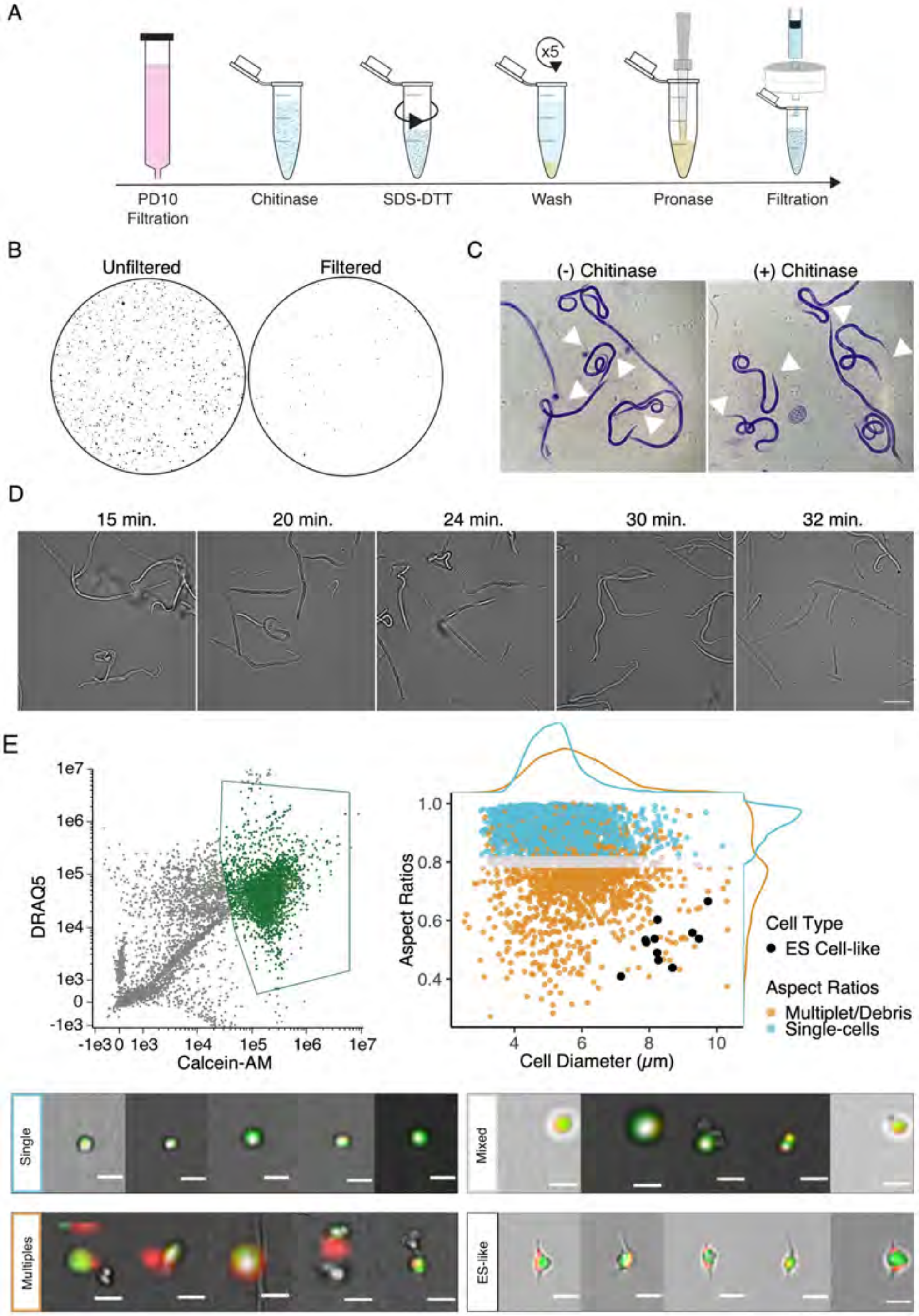

Figure 1. Optimization of single-cell dispersions in *B. malayi* microfilariae.
(**A**) Schematic of dissociation protocol using 1 million *B. malayi* microfilariae as input. (**B**) Pre- and post- PD-10 filtration of microfilariae-containing peritoneal lavage. Unfiltered solutions (left) contain a plethora of host cell and tissue contamination and parasite embryos. Filtered solutions (right) minimize host contamination carryover prior to cell dispersion. (**C**) Representative Giemsa stained microfilariae pre-chitinase (left) and post-chitinase (right) treatment. Chitinase disrupts sheath integrity visible in the head and tail spaces (white arrows). (**D**) Cell dissociation timelapse during pronase digestion and mechanical disruption. Scale bar = 50 µm. (**E**) High content imaging flow cytometry of single-cell suspensions. Objects gated based on nucleation (DRAQ5+ stain) and high viability (Calcein-AM+ stain). Single-cell objects were segregated by IDEAS software and objects with aspect ratios ≥0.8 for brightfield and DRAQ5 channels were counted as single-cells (blue). A mixed population (grey) included objects belonging to doublets/multiples/debris (orange). All captured images were scanned by eye for cells with ES-like morphology (black) and included as single-cells. Scale bars = 10 µm.

High content imaging of cell suspensions confirms capture of rare parasite cell types

The integrity of cells retrieved from *Brugia* mf dispersions was assessed by imaging flow cytometry. A total of 20,000 objects were assessed and 15,683 were identified as debris, undigested worm segments, or nonviable cells as indicated by negative Calcein-AM staining. The remaining 4,317 objects were analyzed using post-acquisition image features to identify 2,893 objects as live, single cells that displayed round cellular and nuclear morphology (**Figure 1E**). While the majority of recovered cells have a diameter of 5.23 ± 0.77 µm, each mf is known to possess a large and morphologically distinct secretory cell that is critical to parasite survival and immune evasion in the host. The *Brugia* secretory cell is hypothesized to be responsible for the release of prominent antigens, extracellular vesicles, and nucleic acids that operate at the host-parasite interface. Classical descriptions of the mf ES system highlight the secretory cell as a large cell with bipolar canal extensions (Moreno et al., 2010; Nelson and Riddle, 1984; Sundaram and Buechner, 2016). We mined cells in our dataset that match this description and identified a total of 11 cells with bipolar appendages that are notably the largest identifiable cells (~8 µm in diameter) in this life stage (**Figure 1E**). Each mf possesses a single secretory cell among hundreds of total cells and this recovery rate (0.4%) falls within the expected range, providing us confidence that our dispersion protocol captures both common and rare cell types.

Single-cell transcriptomic atlas identifies conserved and unique pre-larval cell populations

To define the transcriptional profiles of *B. malayi* microfilariae cell types, we generated a single-cell RNA-seq (scRNA-seq) library from cell dispersions. Dimensional reduction of 46,621 filtered cells via Uniform Manifold Approximation and Projection (UMAP) (McInnes et al., 2018) identified 27 transcriptionally distinct clusters. Across all cells in the dataset, a median of 230 genes and 267 reads per cell were achieved (**Supp. Figure 2**). Transcript abundance of single-cells strongly correlated with microfilariae bulk gene expression (Reaves et al., 2018) (**Figure 2A**, $r = 0.85$, $R^2 = 0.72$, $p = 2.2 \times 10^{-16}$), providing additional evidence that our single cell pipeline largely recapitulates the cell type distribution and transcriptional profile of the intact parasite. Markers for well-characterized *C. elegans* cell types (**Supp. Figure 3**) with one-to-one *B. malayi* orthologs were used to annotate 17 UMAP clusters (**Figure 2A**) totalling 18,317 cells (39.3% of global count). Among these, 6,223 cells were identified as muscle derived (13.3% of global count) and 5,527 cells expressed pan-neuronal markers (11.9% of global count). Additional identifiable clusters include those representing canal-associated cells, coelomocytes, mesodermal tissues, and a pre-alimentary canal related cell type (**Figure 2B**).

Cell types belonging to the mesoderm lineage include 10,284 cells (22% of global count). Body wall muscle cells represent the majority of the mesodermal cells identified (clusters 2 and 19) and are distinctly categorized based on expression of *Bma-hlh-1* (Krause et al., 1994) and markers shown to be enriched in *B. malayi* body wall muscle such as actin and multiple myosins (*Bma-myo-3*, *Bma-unc-54.1*, *Bma-unc-54.2*, *Bma-act-1*) (Morris et al., 2015). An additional two clusters (clusters 9 and 17) strongly express markers associated with mesodermal lineage *C. elegans* cell types (enteric and vulval), including *Cel-hlh-8, Cel-hlh-2*, and *Cel-mls-1* orthologs (Packer et al., 2019; Philogene et al., 2012). Differentially expressed genes between the two clusters are proteins of unknown function and could not be further parsed. Also belonging to the mesodermal cell lineage in *C. elegans* are coelomocytes, phagocytic scavengers located within the pseudocoel. Using coelomocyte-specific *C. elegans* orthologs (*Bma-cup-4*, *Bm6921*, *Bma-unc-122*, *Bma-let-381*), cluster 6 was annotated as coelomocytes. These data show that mesodermal cells in the post-embryonic and pre-larval mf state include well differentiated body wall musculature and coelomocytes and underdeveloped enteric and vulval muscle structures.

Pan-neuronal *C. elegans* markers (*sbt-1, ric-4, ida-1, egl-3, egl-21*) were used to identify nine clusters of putative neurons expressing all five markers (303 genes and 358 reads per cell) (**Figure 2B**). We were able to further resolve a cluster of motor neurons (cluster 11) and interneurons (cluster 23) characterized by one-to-one orthologs of the *C. elegans* motor neuron marker (*Cel-unc-4*) and DVA tail interneuron marker (*Cel-nlp-12*), respectively. Known genes involved in neurotransmitter synthesis and transport were used to map aminergic (cluster 26) and neuropeptidergic neurons (clusters 24 and 25) (**Figure 2C**). Acetylcholine is the primary excitatory nematode neurotransmitter and we used cholinergic pathways genes (*Bma-cha-1*, *Bma-cho-1*, and *Bma-ace-2*) to locate cholinergic neurons. The motor and interneuron neuronal clusters (11 and 23) express *Bma-cha-1* and *Bma-cho-1* in 10-15% of all captured cells. Clusters 3-5 exhibit more abundant expression of *Bma-cha-1* (**Supp. Figure 4**) but no other neuronal markers, cholinergic or pan-neuronal, and may represent a cholinergic neuronal developmental state.

The phylogenetic distance between free-living clade V *C. elegans* and filarial clade III nematodes is associated with known differences in anatomy (Chitwood and Chitwood, 1950) and localization of some orthologous proteins (Moreno et al., 2010), which limits efforts to comprehensively map all cell types across species (**Supp. Figure 5**). Cell types and structures unique to filarial nematodes demand different annotation approaches. A cluster of 503 cells (cluster 22) uniquely displays high expression of chitinases (*Bma-cht-1.1*, *Bma-cht-1.2*, *Bma-cht-1.3*) and the immunomodulatory vaccine candidates *Bma-val-1* and *Bm97.* Chitinase has been shown to be stored in the inner body of microfilariae which is positioned between the excretory and G1 cells and is hypothesized to act as the precursor for the intestinal tract of the developing larvae in the mosquito (McLaren, 1972; Wu et al., 2008). The combination of chitinase and molting proteins within this segregated cluster support the annotation of cluster 22 as inner body-associated cells.

Among *C. elegans* excretory-secretory cell types, only canal-associated cell (CAN) specific markers could be associated with a *B. malayi* single-cell cluster. *B. malayi* orthologs (*Bma-pks-1*, *Bma-acbp-6*, *Bma-ceh-10*) of CAN markers identify cluster 14 as ES canal-associated cells (1,006 total cells). Given the unique cell composition and structural adaptations of the ES system in filarial nematodes, identification of additional secretory cell types demands other approaches.

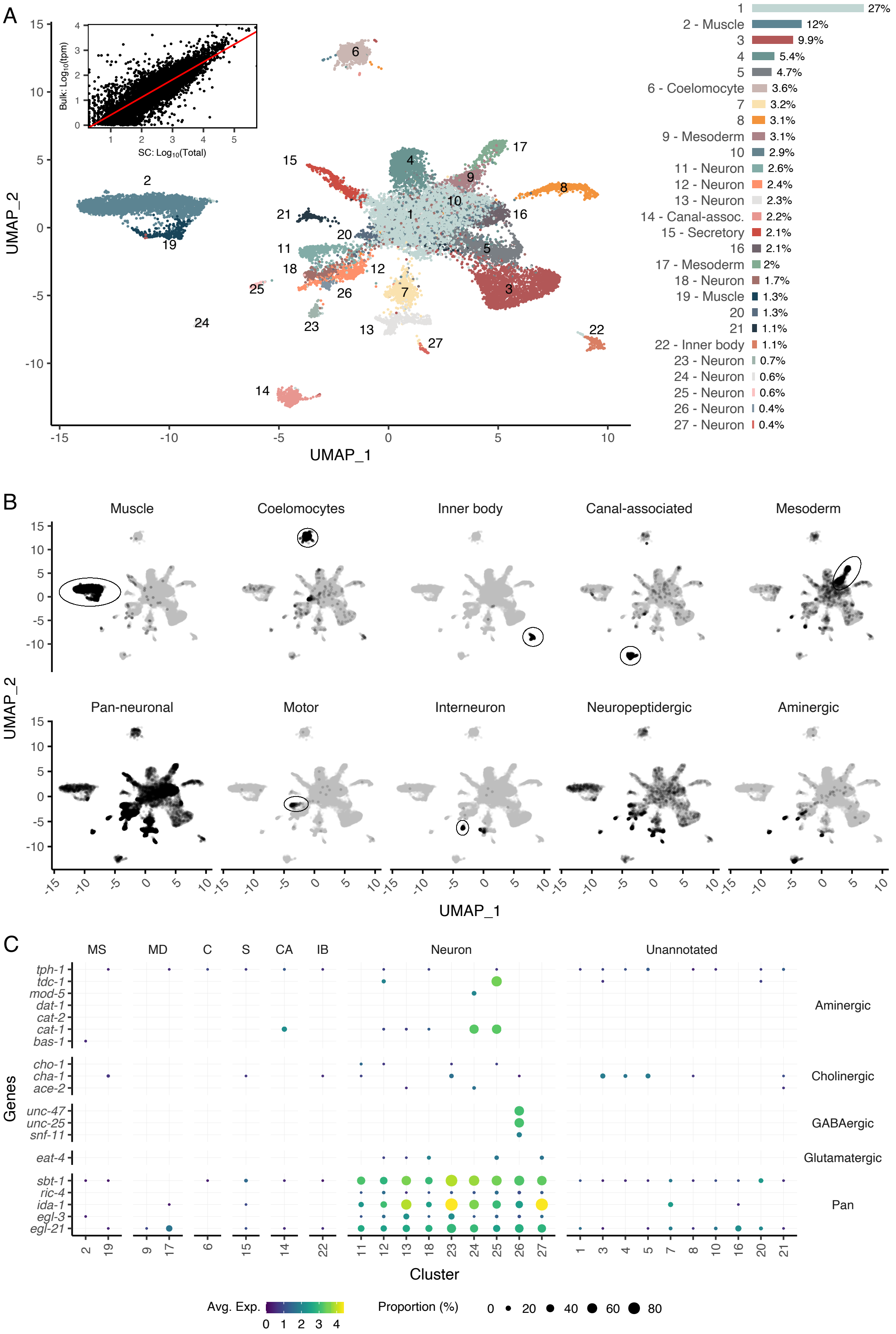

Figure 2. A single-cell transcriptomic atlas of *B. malayi* microfilariae cell types.
(**A**) Global UMAP transcriptome clustering of 46,621 cells. Comparison of bulk transcript per million counts (tpm) (Bulk: Log$_{10}$(tpm)) and single-cell RNA-seq total read counts (SC: Log$_{10}$(Total)) indicates the transcriptomic profile of the single-cell atlas largely recapitulates the gene expression profile of bulk tissue RNA-sequencing (inset). Bars indicate the percent of total cells per cluster. (**B**) Annotation of transcriptomic clusters using *B. malayi* and *C. elegans* cell-type specific markers. (**C**) Gene expression distribution (color) and proportion of cells per cluster (size) expressing neurotransmitter-specific genes.

Identification of secretory-related cell types using FACS and RNA-seq approaches

We exploited the large size of the *B. malayi* secretory cell as a means to enrich for and profile this rare cell type within single-cell suspensions. The largest viable cells within a *B. malayi* microfilariae suspension were FAC-sorted and pooled for downstream RNA-seq (**Figure 3A**). The transcriptional profiles of these outlier cells were compared to smaller round cells that typify the mf cell population, and unique identifiers of the largest cells were mapped to the single-cell atlas UMAP. Cluster 15 shows a clear overall enrichment for the 78 genes more highly expressed in this sorted cell population (**Figure 3B** and **Supp. File 1**) and individual cells within this putative secretory cell cluster represent the largest group coexpressing different subsets of these markers (**Figure 3C**).

To assess whether the *C. elegans* excretory cell would have provided information relevant to unearthing the filarial secretory cell, we carried out pooled single-cell RNA-seq of GFP tagged (*vha-1p::*GFP) and sorted *C. elegans* excretory cells (**Figure 3D** and **Supp. File 2**). Established and new *C. elegans* excretory cell markers identified through this effort lack clear orthologs or display no meaningful overlap with *B. malayi* secretory cell markers (**Figure 3E**). This aligns with the distinct evolutionary history of the ES system in filariae and the parasite-specific functions the secretory cell is likely to perform in the host context.

Abundantly-secreted parasite proteins have diverse tissue origins

We next investigated the origins of prominent molecules known to be secreted by blood-circulating microfilariae and that are likely necessary for parasite immune evasion and survival. Studies have identified secreted proteins and antigens across the intra-mammalian life cycle stages. We mined the literature for a comprehensive list of major antigens, vaccine targets, diagnostic markers, and other notable secreted proteins and probed the scRNA-seq data to identify their transcriptional origins (**Figure 3F**). Transcripts encoding for secreted proteins exhibit variable patterns of expression across the body and very few are specifically localized to the secretory cells (cluster 15). Some prominent antigens that are expressed across many tissue types (*Bma-tpi-1* and *Bma-cpi-2*) have been localized to the ES apparatus via whole-mount antibody staining (Moreno et al., 2010), an observation that is likely reconciled by aggregation and secretion of these proteins through the ES apparatus. Additional broadly expressed antigens that are included as vaccine targets and diagnostic markers include *Bma-tpi-1*, *Bma-sxp-2,* and *Bm3837* (**Figure 3F** and **Supp. Figure 6**) (Krushna et al., 2009; Lalitha et al., 2002; Morris et al., 2013).

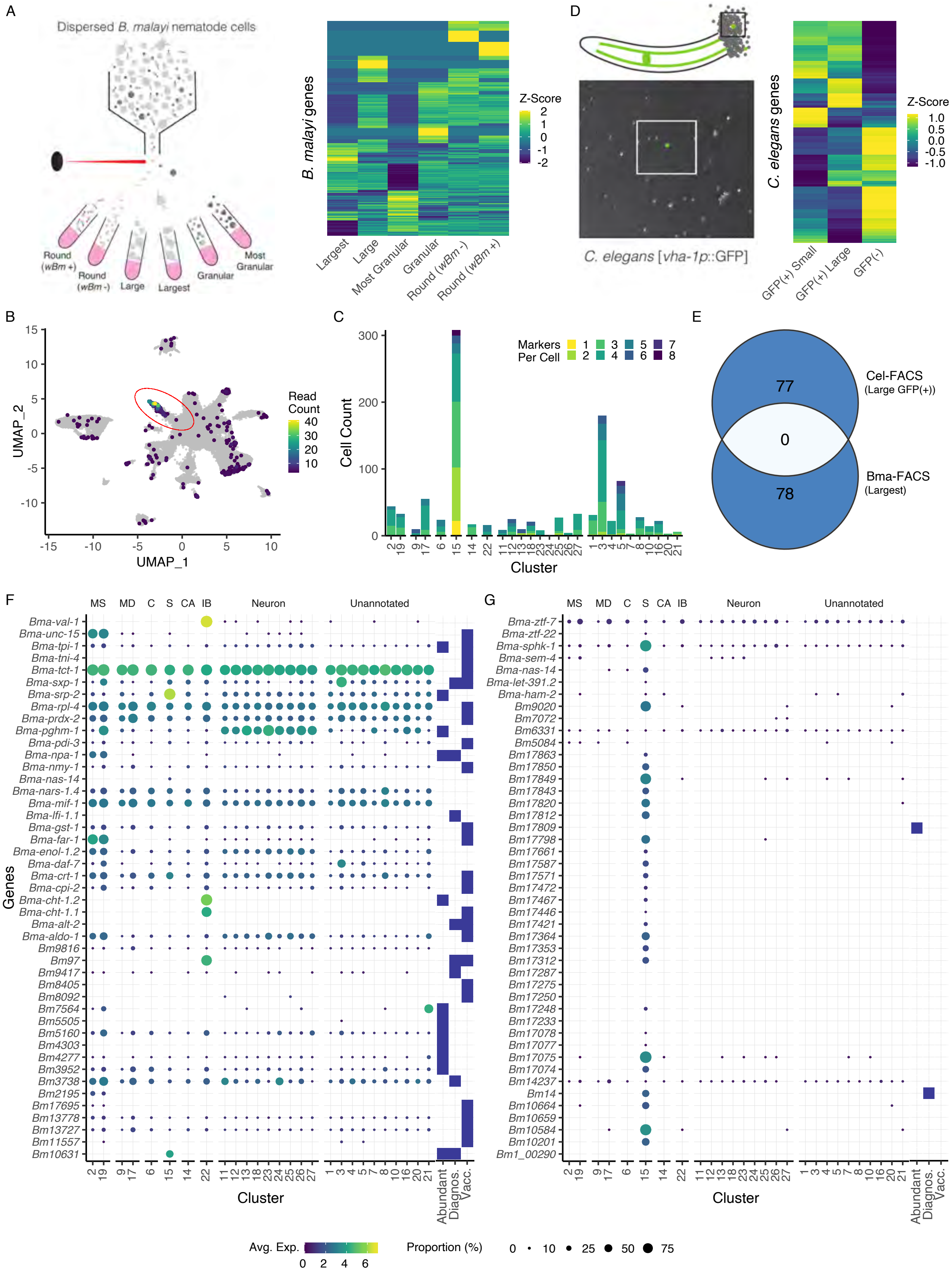
A
Dispersed B. malayi nematode cells
Round (wBm +)
Round (wBm -)
Large
Largest
Granular
Most Granular
B. malayi genes
Z-Score
2
1
0
-1
-2
Largest
Large
Most Granular
Granular
Round (wBm -)
Round (wBm +)
D
C. elegans [vha-1p::GFP]
C. elegans genes
Z-Score
1.0
0.5
0.0
-0.5
-1.0
GFP(+) Small
GFP(+) Large
GFP(-)
B
UMAP_1
UMAP_2
Read Count
40
30
20
10
C
Cell Count
Cluster
Markers Per Cell
1 2 3 4 5 6 7 8
E
Cel-FACS (Large GFP(+))
Bma-FACS (Largest)
77
0
78
F
G
MS MD C S CA IB Neuron Unannotated
Genes
Cluster
Abundant
Diagnos.
Vacc.
Bma-val-1
Bma-unc-15
Bma-tpi-1
Bma-tni-4
Bma-tct-1
Bma-sxp-1
Bma-srp-2
Bma-rpl-4
Bma-prdx-2
Bma-pghm-1
Bma-pdi-3
Bma-npa-1
Bma-nmy-1
Bma-nas-14
Bma-nars-1.4
Bma-mif-1
Bma-lfi-1.1
Bma-gst-1
Bma-far-1
Bma-enol-1.2
Bma-daf-7
Bma-crt-1
Bma-cpi-2
Bma-cht-1.2
Bma-cht-1.1
Bma-alt-2
Bma-aldo-1
Bm9816
Bm97
Bm9417
Bm8405
Bm8092
Bm7564
Bm5505
Bm5160
Bm4303
Bm4277
Bm3952
Bm3738
Bm2195
Bm17695
Bm13778
Bm13727
Bm11557
Bm10631
Bma-ztf-7
Bma-ztf-22
Bma-sphk-1
Bma-sem-4
Bma-nas-14
Bma-let-391.2
Bma-ham-2
Bm9020
Bm7072
Bm6331
Bm5084
Bm17863
Bm17850
Bm17849
Bm17843
Bm17820
Bm17812
Bm17809
Bm17798
Bm17661
Bm17587
Bm17571
Bm17472
Bm17467
Bm17446
Bm17421
Bm17364
Bm17353
Bm17312
Bm17287
Bm17275
Bm17250
Bm17248
Bm17233
Bm17078
Bm17077
Bm17075
Bm17074
Bm14237
Bm14
Bm10664
Bm10659
Bm10584
Bm10201
Bm1_00290
2 19 9 17 6 15 14 22 11 12 13 18 23 24 25 26 27 1 3 4 5 7 8 10 16 20 21
Avg. Exp.
0 2 4 6
Proportion (%)
0 10 25 50 75

Figure 3. Annotation of the *Brugia* secretory cell and localization of secretory-related antigens indicates broad distribution of antigen transcriptional origins.
(**A**) Schematic of FACS enrichment approach for isolating cell populations in *B. malayi* mf single-cell dispersions. Viable cells were sorted by size, granularity and the presence or absence of anti-*Wolbachia* fluorescent antibodies and collected directly into TRIzol LS™ for RNA isolation and sequencing. (**B**) Differentially expressed genes in the "Largest" cells sample, the population hypothesized to contain the secretory cell, were projected on the mf single-cell atlas and indicated expression enrichment in cluster 15. Read count represents summed reads across mapped genes in the single-cell atlas. (**C**) Cell and marker coexpression quantification in cells belonging to cluster 15 using the DEGs identified in Figure 3A. Cluster 15 includes the majority of cells expressing DEGs and contains the most cells coexpressing 1 or more markers. (**D**) Single-cell suspension of *C. elegans* strain BK36 with the excretory canal cytoplasm labeled with GFP. Heatmap representing differential gene expression from sorted cell populations by FACS based on size and GFP(+/-) expression. (**E**) Venn diagram comparing most differentially expressed markers for *B. malayi* mf "Largest" and *C. elegans* "GFP(+) Large" cell populations showing no overlap of orthologous markers. (**F**) Dot plot of secreted, diagnostic, and vaccine antigens grouped by annotated cell type. Color indicates average gene expression per cluster. Circle diameter denotes proportion of cells in each cluster expressing the indicated gene. (**G**) Enrichment of zinc finger C2H2 type transcription factors in the secretory cluster shown by dot plot. Color indicates average gene expression per cluster. Circle diameter denotes proportion of cells in each cluster expressing the indicated gene.

We identified prominent antigens and diagnostic markers that exhibit much more tissue-restricted expression in both secretory and non-secretory cell types. *Bma-val-1*, *Bm97*, and chitinases (*Bma-cht-1.1* and *Bma-cht-1.2*) have strong and nearly undivided expression in the inner body (**Supp. Figure 6**). Muscle and undefined cell types also harbor an abundance of transcripts of interest (ex. *Bma-unc-15*, *Bma-sxp-1*, *Bm7564*). Notable genes that showed strong or exclusive expression in the annotated secretory cells include diagnostic antigen *Bm10631* (*BmR1)* (Greene et al., 2022)*,* microfilariae-specific serpin *Bma-srp-2,* and *Bm14*, a Cys_2His_2 (C2H2) zinc finger transcription factor (**Figure 3F and G**). Of particular interest was the abundance of C2H2 transcription factors localizing almost exclusively to the secretory cells. The C2H2 zinc finger family of transcription factors are understood to be a diverse family of proteins involved in DNA-binding and regulation of transcription (Kang and Kim, 2000; Razin et al., 2012). Previous studies (Bennuru et al., 2011; Choi et al., 2011) have described an enrichment of this transcription factor class in mf-derived ES products and elevated expression of these genes in mf. The role of these proteins in ES cell types is poorly understood, but may involve governing gene regulatory events that help adapt mf for the stark environmental transition from the mammalian host to the mosquito vector.

Mapping anthelmintic targets across the microfilarial body

Modulation of ES processes may explain the mechanism of action of essential anthelmintics (Moreno et al., 2021) and a deeper understanding of the cellular or physiological processes that regulate ES systems may identify new therapeutic strategies. Ion channels and structural proteins in the neuromuscular system are the primary targets of nearly all anthelmintics. To identify the distribution of the known and putative targets of existing and emerging anthelmintics within the microfilarial body, we mapped the cell type locations of β-tubulins, cys-loop ligand gated ion channels (LGICs), and additional ionotropic receptors (**Figure 4A**). Benzimidazoles compromise nematode cell structural integrity by acting as microtubule inhibitors, but the specific β-tubulin target(s) are unknown in filariae despite the use of albendazole (ABZ) in MDA programs. The four β-tubulin *B. malayi* proteins exhibit broad expression across the mf body, with *Bma-btub-1* (*Bm4733)* most highly expressed compared to all other β-tubulins (**Figure 4A and B**). This β-tubulin also has the highest sequence similarity to the benzimidazole target in C. elegans (*ben-1*) and we hypothesize that *Bma-btub-1* is responsible for mediating the antifilarial action of ABZ. *Bma-tbb-4* and *Bma-mec-7* were minimally represented but found in muscle and neuronal cell types. Single-cell coexpression of β-tubulins within individual cells shows strong association between *Bma-tbb-4* and *Bma-btub-1* and a moderate association between *Bma-btub-1* and *Bma-btub-2* (**Figure 4C**), pointing to potential redundancy and compensatory drug response mechanisms.

Transient receptor potential (TRP) channels are gaining recognition as anthelmintic targets (Park et al., 2019) and the TRPC-like channel *Bma-trp-2* has recently been implicated as a target of diethylcarbamazine (DEC) (Verma et al., 2020; Williams et al., 2022). We observed the expression of all 10 *B. malayi* TRP channels with at least one TRP channel subunit expressed in every cell type (**Figure 4A and Supp. Figure 7**). *Bma-trp-2* facilitates inward calcium currents upon activation and results in subsequent opening of the SLO-1 K^+ channel (Verma et al., 2020; Williams et al., 2022), the proposed target of the macrofilaricidal emodepside (Kashyap et al., 2019). The majority of *Bma-trp-2* and *Bma-slo-1* transcripts are found in body wall muscle (clusters 2 and 19), consistent with electrophysiological assays (Kashyap et al., 2019; Verma et al., 2020) and the paralytic effect of emodepside.

The glutamate-gated chloride channels (GluCls) are of special interest as the targets of the macrocyclic lactones and as regulators of ES processes. There is strong evidence that ivermectin (IVM) acts on muscle-expressed GluCls adjacent to the secretory apparatus leading to suppression of secretory cargo and host clearance of mf (Harischandra et al., 2018; Li et al., 2014; Loghry et al., 2020; Moreno et al., 2010). The *B. malayi* GluCl complement (*Bma-avr-14, Bma-glc-2, Bma-glc-3,* and *Bma-glc-4*) display expression in neuronal and muscle cell types (**Figure 4A** and **4B**). *Bma-avr-14* is noted as an important subunit for IVM sensitivity (Dent et al., 2000), and the expression of *avr-14* in annotated muscle cell types is consistent with its expression in muscle surrounding the ES pore (Moreno et al., 2010). While functional *B. malayi* GluCl channels have been constituted in heterologous systems to determine IVM sensitivity (Choudhary et al., 2022; Lamassiaude et al., 2022), not all subunit compositions are amenable to expression and it is unclear what channel formations best reflect the native state (Lamassiaude et al., 2022). To improve predictions of native channel compositions, we examined the correlation of GluCl subunit expression in individual cells and identified *Bma-avr-14* and *Bma-glc-4* as the most commonly coexpressed GluCl subunits (**Figure 4C**). *Bma-avr-14* was also coexpressed with *Bma-glc-2*, a combination reported to be IVM-sensitive, however *Bma-glc-2* was minimally expressed and was not coexpressed with any other GluCl subunit.

Nicotinic acetylcholine receptors (nAChR) are activated by levamisole and other cholinergic anthelmintics. As expected, the subunits that comprise *L*-type and *P*-type nAChR channels are mainly restricted to the body wall muscle (**Supp. Figure 7**). Single-cell coexpression analysis of nAChRs reveals that *Bma-acr-15* could be an essential and missing component of our understanding of nAChR composition and function in filarial nematodes (**Figure 4C**). These data enrich our understanding of tissue-specific targeting of the major anthelmintic classes and provide new cell-specific leads belonging to traditionally druggable receptor families.

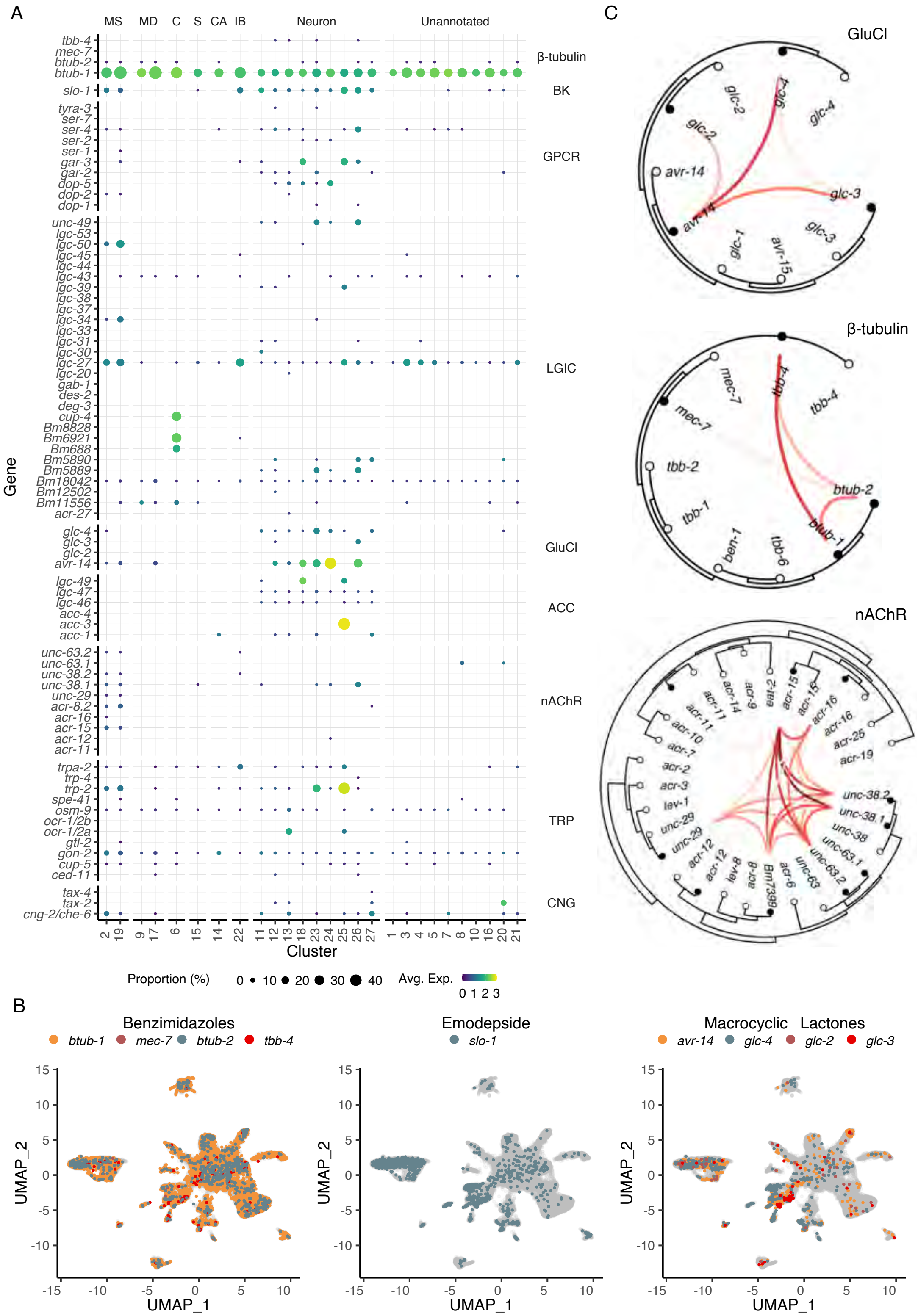

Figure 4. Distribution of putative anthelmintic targets and LGIC subunit colocalization.
(**A**) Transcriptomic and gene expression profiles of major anthelmintic targets in microfilarial cell types. Targets include β-tubulins and cys-loop ligand-gated ion channel (LGIC) subunits corresponding to the following subfamilies: big potassium (BK), G-protein coupled receptor (GPCR), glutamate-gated chloride channel (GluCl), acetylcholine-gated channel (ACC), nicotinic acetylcholine receptor (nAChR), transient receptor potential channel (TRP), and cyclic nucleotide-gated ion channels (CNG). (**B**) UMAP depiction of cells expressing putative targets of benzimidazoles (β-tubulins), emodepside (*slo-1*), and macrocyclic lactones (GluCls). (**C**) Phylogenetic trees showing single-cell correlations between subunits belonging to GluCl and nAChR LGIC subfamilies and β-tubulins. Empty circles represent *C. elegans* and filled circles represent *B. malayi*. Red links indicate positive Pearson correlation coefficients calculated using the log normalized count values.

Measuring the effects of anthelmintics on the viability and transcriptional states of isolated cells.

With a view of how anthelmintic targets are distributed across cells and tissues, we set out to investigate anthelmintic responses at single-cell resolution. To first validate flow cytometry as a cell viability quantification approach, single-cell suspensions from the same *B. malayi* dispersion reaction were exposed to DMSO, methanol (nonviable), or remained untreated (viable). Cell viability was successfully measured using DRAQ5 (nucleated objects) and Calcein Violet-AM, a cell-permeable viability dye that remains within healthy cells after acetoxymethyl (AM) cleavage by non-specific esterase activity (**Figure 5A**). We also confirmed that cell health did not decline significantly after dispersion and incubation on ice in media for up to 8 hr and that DMSO at concentrations required for drug solubility did not compromise cell health (**Figure 5B**).

Next we examined the effects of three major anthelmintic classes (macrocyclic lactones, benzimidazoles, and nicotinic agonists) on parasite cell viability. Homogenous cell preparations from independent parasite infection cohorts were split into parallel treatment conditions and cells were exposed to drugs for a 20 min incubation period prior to flow cytometry analysis. Dose response curves (50 nM, 1 µM, 50 µM, 100 µM) were completed using ivermectin (IVM), levamisole (LEV), and albendazole sulfoxide (AZS), the active metabolite of albendazole (**Figure 5C**). We did not observe a significant decrease in cell viability in any of the primary classes of drug at pharmacologically relevant concentrations, however, higher concentrations of IVM did produce a cytotoxic effect (EC_{50}= 51 µM) (**Figure 5D**).

While these anthelmintics did not exhibit strong cell-cidal activity, we reasoned they may differentially alter gene expression in various cell types. Single-cell RNA-sequencing was carried out using a homogenous *B. malayi* mf cell suspension that was equally split with one half receiving short-term IVM exposure at a concentration that does not affect cell viability (1 µM for 20 min). Compared to the untreated control, muscle, neurons, and unannotated cell types revealed the most significant and abundant upregulation of genes in response to IVM exposure (**Figure 5E** and **Supp. File 3**). The greatest transcriptional shift occurs in muscle cells, which house the highest transcriptional abundance of GluCls (**Supp. Figure 7**). Differentially expressed genes of interest include serine protease inhibitor *Bma-srp-2*, a highly abundant ES product released from mf, which showed the greatest increase in expression in unannotated cluster 8 ($Log_2FC > 2.8$) but was also significantly upregulated in 9 of 27 clusters. The IVM response was additionally characterized by upregulation of genes previously identified in bulk RNA-seq studies (*Bm10661, Bm228, Bm9776, Bma-srp-2, Bm8514, Bma-unc-54.2, Bm33, Bm13260, Bma-rps-28*) (Ballesteros et al., 2016) and proteins with unassigned functions.

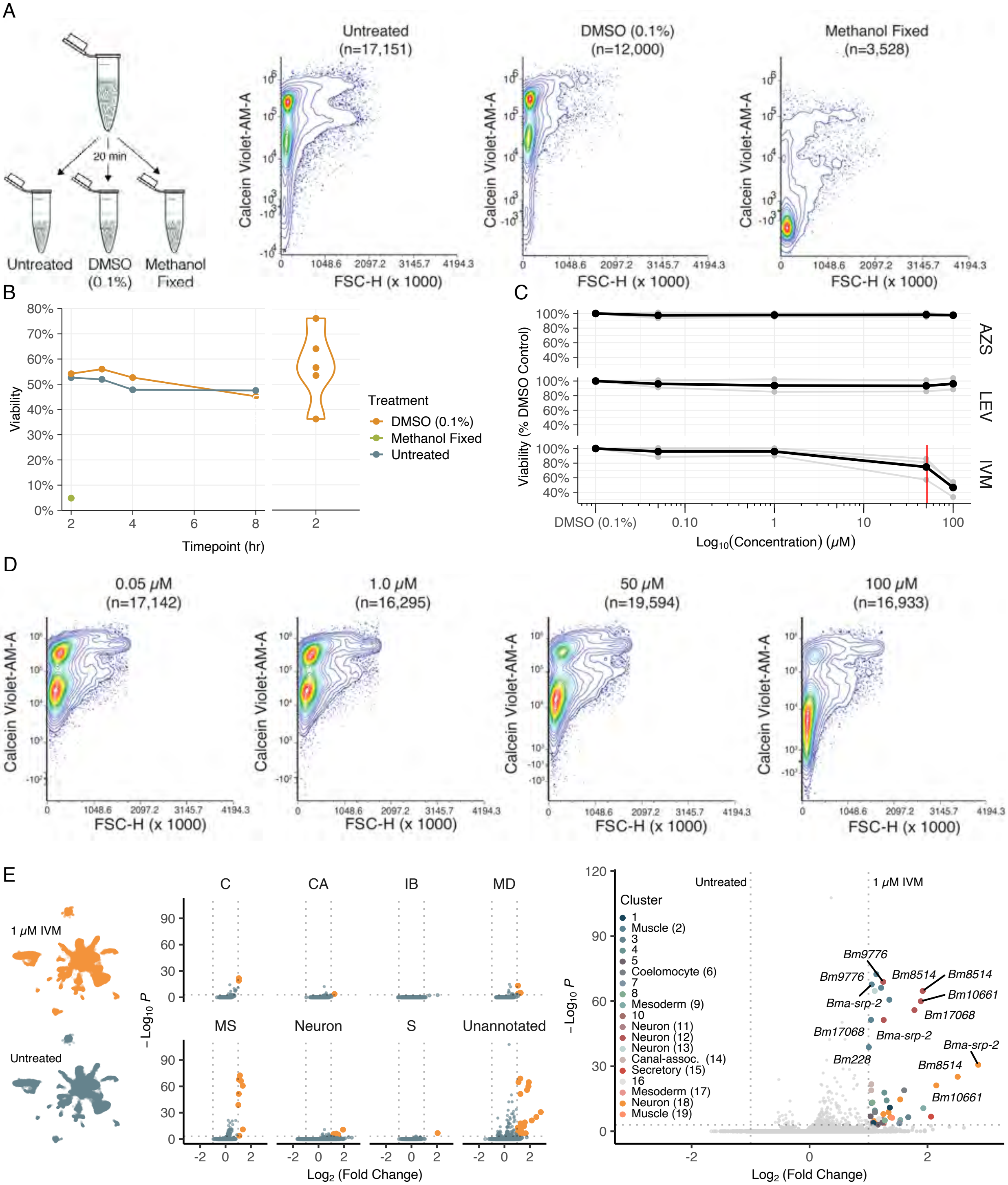
A
20 min
Untreated
DMSO (0.1%)
Methanol Fixed
Untreated (n=17,151)
DMSO (0.1%) (n=12,000)
Methanol Fixed (n=3,528)
Calcein Violet-AM-A
FSC-H (x 1000)
0
1048.6
2097.2
3145.7
4194.3
B
Viability
Timepoint (hr)
Treatment
DMSO (0.1%)
Methanol Fixed
Untreated
C
Viability (% DMSO Control)
AZS
LEV
IVM
DMSO (0.1%)
0.10
1
10
100
Log₁₀(Concentration) (μM)
D
0.05 μM (n=17,142)
1.0 μM (n=16,295)
50 μM (n=19,594)
100 μM (n=16,933)
Calcein Violet-AM-A
FSC-H (x 1000)
E
1 μM IVM
Untreated
C
CA
IB
MD
MS
Neuron
S
Unannotated
−Log₁₀ P
Log₂ (Fold Change)
Untreated
1 μM IVM
Cluster
1
Muscle (2)
3
4
5
Coelomocyte (6)
7
8
Mesoderm (9)
10
Neuron (11)
Neuron (12)
Neuron (13)
Canal-assoc. (14)
Secretory (15)
16
Mesoderm (17)
Neuron (18)
Muscle (19)
Bm9776
Bm9776
Bm8514
Bm8514
Bm10661
Bma-srp-2
Bm17068
Bm17068
Bma-srp-2
Bma-srp-2
Bm228
Bm8514
Bm10661

Figure 5. Cell viability and transcriptional shifts in response to anthelmintics. (**A**) Schematic and representative flow cytometry contour plots depicting calcein violet-AM (viable) fluorescence in control samples (untreated, 0.1% DMSO, and methanol fixed). Methanol fixed cells show no retention of calcein violet-AM indicated by decreased fluorescence in the violet channel. (**B**) Viability of dispersed cell suspensions incubated on ice for 8 hr Significant variation in the percent viability of cell populations after dispersion was observed and attributed to the variation in mf health prior to cell dispersion as well as small nuances in pronase digestion. (**C**) Drug dose response curves on dispersed single-cell suspensions at 50 nM, 1 µM, 50 µM, 100 µM, and a DMSO-only (0.1%) control. Viability was normalized to the percent DMSO control. Black line indicates the average of three replicates. AZS = albendazole sulfoxide, LEV = levamisole, IVM = ivermectin. Red line indicates the EC_{50} value for IVM at 51 µM. (**D**) Representative flow cytometry contour plots of cell viability in response to IVM treatment. A decrease in calcein violet-AM fluorescence at 50 µM and nearly total cell death at 100 µM. (**E**) Left: Single-cell transcriptomic response to IVM treatment (1 µM for 20 min, 1% DMSO). UMAP plot showing treated (top) and untreated (bottom) clustering of cell types. Middle: Volcano plots depicting differentially expressed genes in treated and untreated groups by cell type annotations. Orange color indicates upregulation in IVM-treated cells. Right: Volcano plot of differentially expressed genes colored by cluster.

Cell culture of dispersed mf suspensions provides avenue for single-cell functional analyses

Historically, cell culture models have revolutionized biological understanding and progress towards drug discovery and development in mammalian systems. The complex cyclodevelopmental life cycle of filarial worms and the absence of immortalized cell lines derived from any helminth species complicate the translation of these approaches to helminthology. While dispersions of embryonic *Brugia* cells have been performed, the captured cells do not differentiate in culture (Higazi et al., 2004), limiting the advantages of the system. To enable future studies of cell biology and drug interaction at single-cell resolution, we sought to establish a filarial nematode cell culture system for the longer-term maintenance of adherent and differentiated cell populations. To this end, *B. malayi* mf primary cell cultures were plated onto peanut-lectin coated chamber slides and imaged to assess cell adherence and health. Highly viable populations of adhered cells were observed after a 24 hr incubation in 10% FBS L-15 media (**Figure 6A**). We next plated primary cells onto peanut-lectin coated surfaces in microtiter plate format to monitor viability over a longer time frame using high-throughput imaging. Adhered cells remained viable at 42 hr as indicated by Calcein-AM fluorescence (**Figure 6B**). Further development and adaptation of this method will support functional studies of differentiated *B. malayi* cell populations.

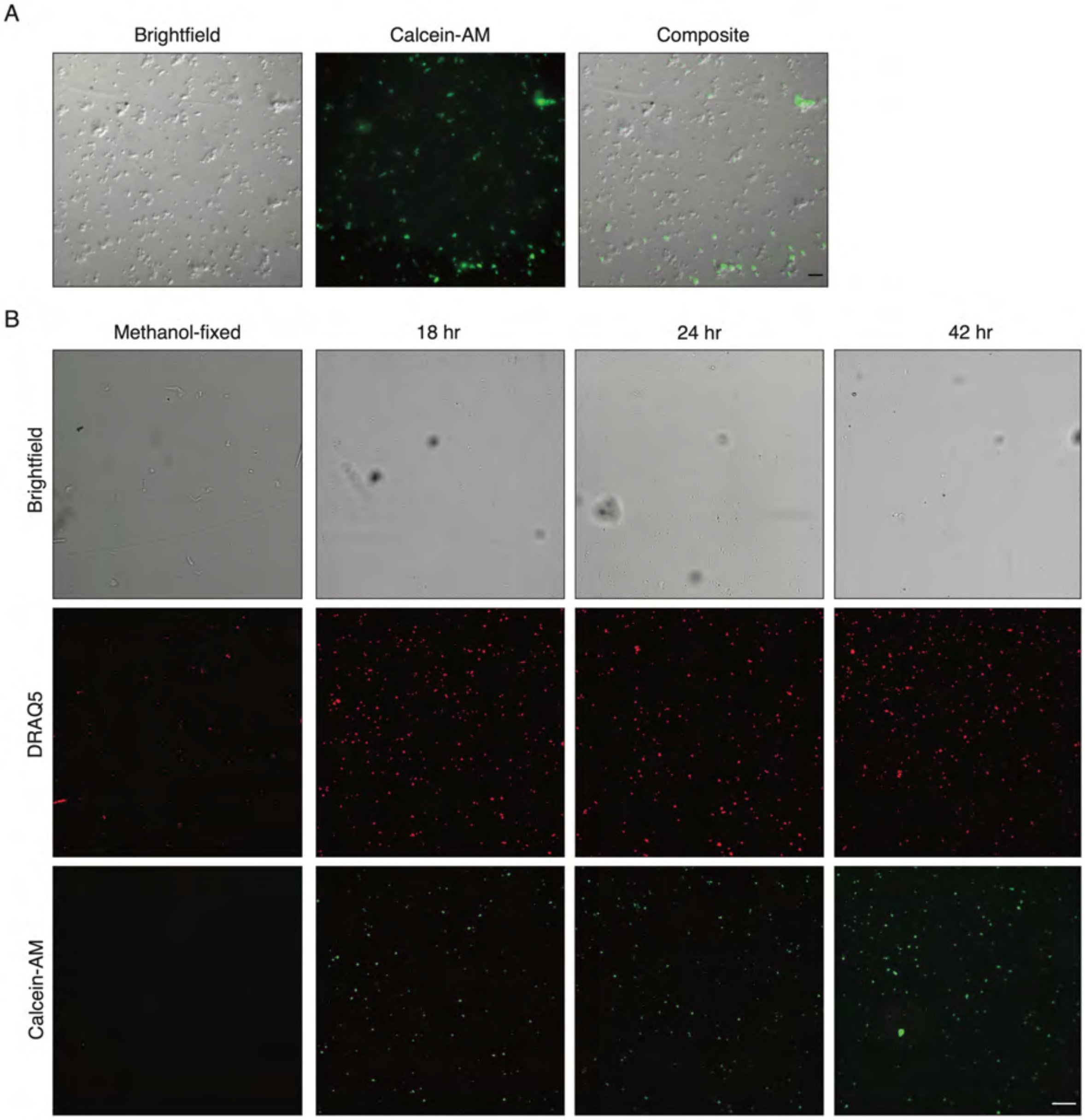

Figure 6. Cells of dispersed microfilarial are viable in culture 42 hr after dispersion.
(**A**) DIC and fluorescence microscopy of cells from microfilarial stage *B. malayi* parasites on peanut-lectin coated slides after 24 hr incubation in culture medium. The cell population contains a range of cell sizes including single-cells and clustered cells and a subset of the cell population have protrusions indicating a muscle or neuronal cell type. Calcein fluorescence (live) with varying intensities of brightness indicates a range of viability among the cell population. Scale bar is 20 µm. (**B**) Brightfield and fluorescence microscopy of cell viability over a period of 42 hr using DRAQ5 and Calcein-AM viability dyes. Methanol-fixed cells served as a control for non-viable cells and lack expression in the GFP channel used to measure Calcein fluorescence. A 0 hr timepoint could not be imaged due to the requirement of adherence to peanut lectin for high resolution imaging, however flow cytometry and image stream data confirm reliable viability of dispersed cells. Expression of calcein in cells at 42 hr indicates cells can remain viable in culture for up to 42 hr Scale bar is 50 µm.

Discussion

Excretory-secretory products released by parasitic nematodes into the host environment are recognized as key molecular mediators for the establishment and maintenance of infections. The secretory processes that underlie host immune evasion and modulation may serve as targets for existing (Loghry et al., 2020; Moreno et al., 2010) and future drugs. Despite this, our superficial knowledge of the structure and function of the secretory apparatus of human parasitic nematodes has limited our understanding of the molecular events that drive host-parasite interactions. To help address these knowledge gaps, we introduce the first single-cell transcriptomic atlas of a parasitic nematode and leverage this resource to resolve tissue and cell-specific gene expression patterns that allow for inferences about the origins of secretory products and antiparasitic mechanisms of action.

We developed a single-cell dispersion and RNA-seq protocol to generate a transcriptomic atlas of the blood-circulating microfilariae stage of the human filarial parasite *Brugia malayi*. Using marker genes specific for terminal and developmenting cell types, we annotated ~30% of the cells represented in our dataset as muscle and neuronally derived. Ten clusters in the dataset (61.5% of total cell count) remain unannotated. The use of a pre-larval developmental stage containing cells that have yet to terminally differentiate and a developmentally asynchronous mf population likely contributed to difficulties in comprehensive disentanglement and annotation of transcriptionally distinct cell clusters. The potential to annotate cells is further confounded by the unknown biological functions of genes that distinguish different clusters. Many unannotated clusters in the dataset may be resolved by deeper single-cell profiling and validation efforts. For instance, cluster 7 lowly expresses several *C. elegans* genes found in sensory neurons related to cilium assembly and organization (*osm-1, dyf-11, ccep-290, ift-74, dyf-17, che-3, T12B3.1*) (Inglis et al., 2006) but lowly expressing only a subset of pan-neuronal markers.

Knowledge from *C. elegans* was useful in identifying rare cell populations such as coelomocytes or canal-associated cells, but alternative approaches were necessary for the identification of clade-diverged secretory cells. Pooled RNA-seq of sorted cell populations enriched for the morphological characteristics of the *B. malayi* secretory cell allowed for the annotation of secretory-like cells within the mf cell atlas. Surprisingly, prominent secreted proteins and antigens show different patterns of transcript distribution across cell populations, establishing that immunomodulatory ES products originate from different parasite tissues. For example, the diagnostic marker *BmR1* (*Bm10631)* is exclusively transcribed in the secretory cell while the vaccine immunogens *Bma-val-1* and *Bm97* are restricted to the inner body. It is possible that many of the proteins encoded by these transcripts share a common exit route from the worm through the ES apparatus (Moreno et al., 2010).

The inner body is a chitinase-enriched (*Bma-cht-1.1, Bma-cht-1.2*) intestinal tract precursor, and its breakdown leads to the release of chitinase and exsheathment within the mosquito (Wu et al., 2008). Exposure of mf to IVM prevents later exsheathment in the mosquito (U. R. Rao, A. C. Vickery, B. H. Kwa, J. K. Nayar, 1992), which we speculate is consistent with suppression of ES function leading to the trapping of inner-body enzymes. This view of the mf ES apparatus as a secretory choke point in the parasite life cycle offers a control target relevant to both the arthropod and mammalian hosts. Later developmental stages in the parasite life cycle (L3 and adults) present additional orifices and interfaces for host interaction, necessitating other approaches to parse out the relationship between ES products and the ES apparatus in these stages.

The putative targets for mainstay anthelmintics are known, but their tissue distributions throughout the filarial worm body are unresolved. Further, the native subunit compositions of the ion channel drug targets of the macrocyclic lactones and nicotinic agonists are unknown. We leveraged these data to map the expression of known and putative antifilarial drug targets across cell types and to predict ion channel subunit associations from single-cell coexpression analysis. These predictions can guide the reconstitution and functional expression of pharmacologically relevant ion channels in heterologous studies of channel function and anthelmintic responses. We directly assessed the effects of anthelmintics on the viability of isolated cells, showing that the major anthelmintic classes do not elicit cell death at pharmacologically relevant concentrations. This suggests that the primary action of these drugs requires cell-cell connectivity. The action of ivermectin in *C. elegans* is innexin-dependent (Dent et al., 2000), underscoring the importance of gap junctions in the signaling cascade that results in the whole-organism drug effect. To capture early transcriptional events that drive IVM action in the mf stage, we identified core genes that are upregulated across isolated cell types in response to acute drug exposure. Future studies that compare the transcriptional trajectories of cells exposed to drug before and after dispersion may help resolve the role of cell-cell communication and various compensatory responses in anthelmintic mechanism of action.

Finally, we developed a protocol for culturing cells derived from *B. malayi* microfilariae cell dispersions. Efforts that improve our ability to manipulate these dispersed cell populations have the potential to expand our understanding of parasite cell biology and receptor-mediated responses to external drug and chemical stimuli. While there has been great progress in the genetic manipulation of filariae (Higazi et al., 2002; Liu et al., 2020, 2018; Xu et al., 2011), germline transgenesis has proven difficult and optimized protocols cannot overcome a two-host life cycle with a long parasite pre-patent period. Transfection of cultured *Brugia* mf primary cells with promoter-driven constructs and CRISPR reagents can help circumnavigate some existing limitations and facilitate the study of parasite protein function. Collectively, the continued development of these resources and associated methods can help answer outstanding questions about the nematode parasite-host-drug interface.

Materials and Methods

Data and Code Availability

All data and scripts used for data analysis and visualization are publicly available at https://github.com/zamanianlab/Bmsinglecell-ms. Single-cell and FACS-pooled RNA-seq data has been deposited into NIH BioProjects PRJNA874113 and PRJNA874749.

Parasite and *C. elegans* Strains

Brugia microfilariae (mf) were supplied by the NIH/NIAID Filariasis Research Reagent Resource Center (FR3) (Michalski et al., 2011). Mf extracted from the jird peritoneal cavity were filtered and cultured in RPMI-1640 with L-glutamine (Sigma-Aldrich, St. Louis, MO) supplemented with 10% fetal bovine serum (FBS) (Thermo Fisher, Waltham, MA) and 50 µg/mL penicillin/streptomycin (P/S) (Thermo Fisher, Waltham, MA). All experiments used mf incubated at 37°C+5% CO_2 for at least 1 hr prior to experimentation within 24 hours of host extraction, or stored at 4°C overnight in fresh media and processed within 48 hours of host extraction. *C. elegans* strain BK36 was acquired from the *Caenorhabditis* Genetics Center (CGC). N2 and BK36 strains were maintained at 20ºC on NGM plates seeded with *Escherichia coli* OP50. Worms were propagated by routine picking of L4 stage worms to seeded NGM plates.

Microfilariae Purification

Brugia malayi mf were purified using a PD-10 desalting column (Cytiva, Marlborough, MA) to remove host cells, debris, embryos, and perished microfilariae as previously described (Galal et al., 1989) with minor changes. Briefly, the PD-10 column was equilibrated by passing 25 mL of RPMI-1640 with L-glutamine through the column. Mf were centrifuged at 2,000 rpm for 10 min and the supernatant was drawn off leaving 5 mL of peritoneal fluid and the mf pellet. Mf were resuspended and the entirety of the suspension was transferred to the equilibrated PD-10 column. RPMI-1640 medium was added to the column in 5 mL increments, and the flowthrough was checked every 5 mL for the presence of mf and host peritoneal cells. Mf were collected when no host peritoneal cells were present in the flowthrough and until mf were no longer being eluted. Recovered mf were washed twice in RPMI-1640 by centrifugation, resuspended in RPMI-1640, and allowed to recover at 37°C for at least one hour prior to beginning a single-cell dispersion.

Microfilariae Single-cell Dissociation

PD-10 column purified mf were used as input for *B. malayi* single-cell dispersions at ~1 million mf per reaction. The mf were aliquoted to a 1.5 mL microcentrifuge tube, pelleted, and resuspended in 2 mg/mL chitinase from *Streptomyces griseus* (Sigma-Aldrich, St. Louis, MO) and incubated at 37ºC with light agitation for 20 min. mf were washed once with 1 mL RPMI-1640 medium and the chitinase-treated pellet was resuspended in SDS-DTT (200 mM DTT, 0.25% SDS, 20 mM HEPES, pH 8.0, 3% sucrose) diluted 1:4 in Leibovitz's L-15 medium without phenol red (Gibco, Waltham, MA) and an adjusted osmolality of 340 mOsm using 1M sucrose. 200 µL of diluted SDS-DTT was added to the mf pellet and placed on a notator for 6 min, where the mf are alive but not thrashing. 1 mL of L-15 medium was added to the tube and centrifuged at 16,000 rcf for 30 sec at 4ºC. The supernatant was removed and the pellet was resuspended in 1 mL fresh L-15 medium. The mf were washed a total of 5 times or until the smell of SDS-DTT was no longer lingering. The pellet was resuspended in 100 µL pronase from *Streptomyces griseus* (VWR, Radnor, PA) at a concentration of 15 mg/mL in L-15 medium (340 mOsm). The reaction was continuously pipetted 100 times every 5 minutes either manually or by the use of the Repetitive Pipettor robot. The reaction was monitored by eye by checking small aliquots throughout the digestion. The reaction was stopped with ice cold 1 mL L-15+10% FBS when most mf were broken open and single-cells were clearly visible in the background (~30 min). The dispersed cells and remaining worms and debris was pelleted by centrifugation at 1,000 rcf for 6 min at 4ºC. The pellet was resuspended in 1 mL cold L-15+10% FBS and centrifuged briefly for 5 sec at 1,000 rcf to separate remaining large debris and single-cells. The top ~900 µL of cell suspension was drawn up into a 1 mL syringe and pushed through a reusable syringe filter (Millipore, Burlington, MA) containing 7 µm mesh (Component Supply, Sparta, TN). The filtrates were combined and used in downstream applications. A standard hemocytometer was the most cost and time effective cell count estimation method with the caveat that differentiating cell versus debris was very difficult. Comparisons between the methods can be found in the supplemental material (**Supp. File 5**).

Imaging Flow Cytometry

Single-cell suspensions maintained on ice were incubated with DRAQ5 (500 nM) (Biolegend, San Diego, CA) and Calcein-AM (500 nM) (Biolegend, San Diego, CA) in L-15+10% FBS for a minimum of 20 min on ice prior to acquisition. An Amnis ImageStream Mark II Imaging Flow Cytometer equipped with a 60X objective and a 2-laser (488 nm and 642 nm), 6-channel detection system was used for single-cell imaging acquisition. Samples were gated based on viability (DRAQ5+, Calcein-AM+). Analysis of images was completed using the Amnis Image Data Exploration and Analysis Software (IDEAS) and the integrated Feature Finder Wizard to distinguish viable single-cells from the population based on a subset of hand-picked single-cells as a training dataset.

Anthelmintic Drug Dose Responses

Single-cell suspensions generated from *B. malayi* microfilariae were subjected to drug treatment using ivermectin (IVM) (Fisher), albendazole sulfoxide (AZS) (Fisher Scientific, Hampton, NH), and levamisole (LEV) (VWR, Radnor, PA). Drugs were suspended in DMSO (Santa Cruz Biotechnology, Dallas, TX) and added to cell suspensions at 50 nM, 1 µM, 50 µM, and 100 µM for 20 min on ice with a final DMSO concentration of 0.1%. At the completion of incubation, the cell suspensions were centrifuged at 1,000 rcf for 6 min and as much supernatant as possible was removed without disrupting the pellet. Cells were resuspended in 300 µL of L-15+10% FBS containing DRAQ5 (2.5 µM) and Calcein Violet-AM (0.75 µM) and stored on ice until flow cytometry analysis. Treatment controls included untreated and DMSO only (0.1%) treated cell suspensions. Controls for spectral flow cytometry included L-15+10% FBS, unstained cells, and DRAQ5 (2.5 µM) and Calcein Violet-AM (0.75 µM) fluorescence minus one controls. Additional controls of L-15+100 µM IVM and unstained cells+100 µM IVM were necessary to confirm the presence of IVM precipitation at high concentrations picked up by the spectral flow cytometer. Viability curves of single-cell suspensions over time were generated using cells from a *B. malayi* mf dispersion (input of ~1 million mf) and split to create three treatment groups (untreated, 0.1% DMSO, and methanol fixed) with four samples each to cover four timepoints over 8 hr. Samples were stained with DRAQ5 and Calcein Violet-AM 30 min prior to analysis on the flow cytometer. Methanol fixed cell suspensions served as a cell death control and were prepared by adding 300 µL methanol (chilled to -20ºC) to 100 µL cell suspension and incubated at 4ºC for 30 min prior to staining and analysis. Samples were analyzed on a Cytek Aurora Spectral Cytometer equipped with five lasers (355 nm UV, 405 nm Violet, 488 nm Blue, 561 nm Yellow-Green, and 640 nm Red). The laser light channels include a forward scatter and side scatter off of both the blue and violet lasers and has 64 fluorescence channel detectors. Selection of single-cell entities was completed using FSC-A vs FSC-H followed by selection of cells that are DRAQ5(+) and Calcein Violet-AM(+). Percent viability was calculated by dividing the Calcein Violet-AM(+) population by the total DRAQ5(+) population.

10x Genomics Preparation and Sequencing

A *B. malayi* mf single-cell dispersion was split into two equal parts and one part was treated with 1 µM ivermectin in DMSO (1.0% final v/v) for 20 min on ice. At the end of incubation, the cells were centrifuged at 1,000 rcf for 6 min at 4ºC, the supernatant was removed, and the cells were resuspended in L-15+10% FBS. Cells were normalized to 1,400 cells/µL as estimated by standard hemocytometer (INCYTO, Cheonan-si, South Korea) to target an input of 12,000 cells for capture on the 10x Genomics Chromium controller. The 10x Genomics 3' Single Cell RNA-seq protocol (v3.1 NextGEM User Guide Rev.D) was followed to generate the gel bead-in-emulsions (GEMs) and post cDNA amplification cleanup. The cDNA library was prepared using the Chromium Dual Index TT primers and the Single Cell 3' v3.1 Reagents and user guide. The library was sequenced on an Illumina NovaSeq6000 to generate ~550 M reads across control and drug-treated samples (2x50 bp on S1 flow cell).

scRNA-seq Mapping

The ivermectin treated and untreated *B. malayi* mf scRNA-seq data were mapped and processed independently. Single-cell RNA-seq data were mapped to the *Brugia malayi* reference genome (Wormbase, WS285) using 10x Genomics Cell Ranger 5.0.1 analysis pipeline. The 10x Genomics 3' Single Cell RNA-seq protocol is strongly biased towards the 3' regions of mRNA which are not well annotated in *B. malayi* thus requiring a modified reference genome to improve the mapping rates of the scRNA-seq data. The 3' UTRs were artificially extended by 50, 100, 150, 200, 250, 300, 400, and 500 bp as previously described with modifications (Taylor et al., 2020). Briefly, the scRNA-seq data was mapped using the Cell Ranger pipeline for each iteration and the total reads for each gene in every iteration were summarized across all of the cells. The gene counts for each extension were normalized to the gene count of the 500 bp extension and the optimal extension length for each gene was determined by identifying the extension that provided at least a 90% increase in mapping rate. The *B. malayi* scRNA-seq raw data was mapped one final time using the newly generated reference genome containing the optimal 3' UTR extension length for each gene. The Cell Ranger filtered output drastically underreported the estimated cell count and is not optimized for small, low expressing cells. Therefore the raw Cell Ranger output was used for filtration and preprocessing.

scRNA-seq Bioinformatics Analysis

The raw Cell Ranger barcode matrix output for each scRNA-seq dataset was filtered to remove empty droplets using the cluster-based R package scCB2 (Ni et al., 2020). Using EmptyDrops (ED) as a scaffold, scCB2 increases the power to distinguish real cells from background empty droplets as well as low-expressing, small cells by pooling low-count barcodes with similar gene expression patterns. The cluster is then compared against the estimated background population to identify irrelevant barcodes. This method of empty droplet filtration allows for the identification of small, low-expressing cells which are prevalent in the *B. malayi* mf single-cell dispersions. The filtered cell population was then used as input into the R package SoupX (Young and Behjati, 2020) to estimate the contribution of cell free mRNA contamination captured in each droplet. Because SoupX can provide a better estimate of contamination when cluster information is supplied, the scCB2-filtered datasets were taken through the Seurat pipeline (Hao et al., 2021) to identify clusters. The raw and clustered datasets were used as input to SoupX and the estimated contamination fraction for the untreated and treated datasets were calculated to be approximately 0.13 and 0.10 respectively. The ambient mRNA contamination was removed and additional filters were applied on the remaining cell population. Cells with high mitochondrial representation (greater than or equal to 10% of all UMIs per cell) were identified using the mitochondrial markers *Bm5157, Bma-nduo-4,* and *Bma-ctc-1 (Qing et al., 2021)*. Cells were removed from the population if a single gene represented greater than or equal to 15% of the total cell transcripts, had greater than 2,500 total genes expressed, and more than 1,800 transcripts. The remaining count matrices for the untreated and treated datasets contained > 10,000 genes with 21,131 and 25,490 cells respectively. Seurat 4.1.1 was used for downstream integration and normalization. First, each matrix was normalized and the top 2,000 variable genes were identified using the NormalizeData() and FindVariableFeatures() functions. Variable genes were then used to integrate the control and treated datasets using the FindIntegrationAnchors() and IntegrateData() functions. Principal component analysis for dimension reduction was completed for clustering and visualization of the combined datasets.

C. elegans Single-cell Isolation

Chunks (~5 mm^2) of media from 4 day old plates were excised by flame sterilized spatula, transferred to 5-10 new 10 cm plates, and incubated at 20ºC. At 102-120 hr post chunking, worms were washed off plates with 15 mL M9, pelleted (~1,100 rpm / 5 sec), and exposed to 6 mL of freshly prepared bleaching solution (20% NaOCl, 0.5 M NaOH in ddH_2O) with mild rotation until partially degraded bodies were observed (6-8 min) under Stemi 508 stereo-microscope. Eggs were pelleted (~1,100 rpm / 5 sec) and washed 3 x in 15 mL M9 media. After the final wash embryos were resuspended in 2-4 mL M9 and counted in 5 x 5 µL droplets on a glass slide under a Zeiss Stemi 508 stereo-microscope. 2,000-4,000 embryos were plated in 125-150 µL M9 on 20 (N2) or 55 (BK36) 10 cm NGM plates seeded with OP50 and kept at 20°C for 46.5 hr prior to single-cell isolation. Single-cells were isolated from synchronized *C. elegans* N2 and BK36 L4 stage worms using an established protocol with modifications (Kaletsky et al., 2016). Worms were transferred in ~30 mL M9 media to 3 x 1.5 mL centrifuge tubes by sequential pelleting by microfuge followed by washing 5 x in 1.5 mL M9. Worms were washed once in 500 µL lysis buffer (200 mM DTT, 0.25% SDS, 20 mM HEPES pH 8.0, 3% sucrose) then incubated for a further 8 min in lysis buffer with continuous rotation. Digested worms were washed 5 x in M9 then subject to 500 µL pronase (20 mg/mL from *Streptomyces griseus* in L-15 for 14-15 min at RT with semi-continuous pipetting. Pronase treatment was stopped with FBS (3% final v/v). Large debris was pelleted by microfuge and cells were filtered (7 µm nylon mesh), stained with 0.5 µg/mL DAPI, and kept on ice. Throughout the protocol samples were checked under stereo and fluorescent microscopes to determine the release and integrity of cells.

FACS Pooled RNA-seq

FACS was performed using a FACS Aria II (Becton Dickinson) for both *C. elegans* and *B. malayi* cell dispersions. *C. elegans* BK36 (Mattingly and Buechner, 2011) single-cell dispersions were sorted directly into TRIzol^{TM} LS (Invitrogen, Waltham, MA) in 1.5 mL microfuge tubes. N2 strain cells were used as reference. Gates included dead cells (DAPI+, 4′,6-diamidino-2-phenylindole, 0.5 µg/mL), GFP+ cells (green fluorescent protein), and cell size by aspect ratios, respectively. Total RNA was purified using Direct-zol RNA Microprep kit (Zymo Research, Irvine, CA), eluted in a minimal volume of nuclease-free water and flash frozen in liquid nitrogen or dry ice and stored at -80ºC. RNA integrity was determined by Agilent RNA 6000 Pico Kit (Agilent, Santa Clara, CA) on a 2100 Bioanalyzer (Agilent) before library preparation. Total RNA was converted to double stranded cDNA and amplified using SMART-Seq v4 (Takara, Kusatsu, Shiga, Japan). Full length cDNA was quantified by 2100 Bioanalyzer (Agilent). 150 pg of amplified cDNA was tagmented and index-amplified using Nextera XT adapters (Illumina). Library quantity was assessed by Qubit HS DNA and quality assessed by 2100 Bioanalyzer (Agilent). Libraries were then balanced and 2x75 bp sequencing was carried on the Illumina MiSeq.

For *B. malayi* single-cell dispersions, gates were set to collect live single-cells (DRAQ5+, DAPI-) based on size (small, large, largest), granularity, and presence or absence of *Wolbachia* antibody. Presence of *Wolbachia* identified by fluorescent conjugated (Lightning-Link® R-Phycoerythrin Conjugation Kit #703-0030) *Wolbachia* surface protein *wBm*0432 / GenPept: WP_011256630 mouse monoclonal antibody (BEI Resources, Manassas, VA). Cells were sorted into 750 uL TRIzol^{TM} LS and libraries were prepared using the NEBNext Single Cell/Low Input RNA Library Prep Kit for Illumina (NEB, version 3.0, #E6420L) and NEBNext Multiplex Oligos for Illumina (Index Primers Set 1, NEB, #E6440G), followed by 2x150 bp sequencing on the Illumina MiSeq.

Microfilariae Cell Culture

Single cell dispersions for the purpose of cell culture were prepared as previously described with the exception of the pronase digestion step. After the initial 30 min incubation with mechanical digestion, the suspension was briefly centrifuged at 1,000 rcf to pellet undigested worms. The supernatant was removed and supplemented with 1 mL L-15+10% FBS and placed on ice to inhibit further pronase digestion on released single-cells. The worm pellet was resuspended in an additional 100 µL of pronase (15 mg/mL) for continued digestion for 30 min with manual pipetting to release cells from worms in early stages of digestion. At the end of pronase digestion, all microcentrifuge tubes were centrifuged at 1,000 rcf for 6 min at 4ºC to pellet undigested material and single-cells. The supernatant was replaced with L-15+10% FBS, tubes were briefly centrifuged(~5 sec) and the supernatant was filtered through 7 µm mesh. Peanut lectin-coated chamber slides or plates were prepared by incubating peanut lectin (0.5 mg/mL) (Sigma-Aldrich, St. Louis, MO) suspended in water in chamber slide wells for 30 min, removed, and allowed to dry while being UV treated for 2 hr for sterilization. Filtered cell suspensions were concentrated prior to plating on peanut lectin-coated chamber slides or plates by centrifugation and resuspension in a smaller volume. Cells were seeded and incubated in a humid chamber at 37ºC+5% CO_2 . Viability was visualized using live/nucleated cell staining with DRAQ5, DAPI, or Calcein-AM dyes.

Microscopy

Differential Interference Contrast (DIC) imaging was completed using an upright Zeiss Axio Imager.D1 microscope equipped with a 100X oil objective (Plan-Neofluoar 100x, NA = 1.3 , Zeiss). All other brightfield and fluorescence microscopy used an ImageXpress Nano Automated Imaging System (Molecular Devices) with 10X and 40X air objectives.

Integrating Model Nematode Datasets

In an effort to identify cell types within the *B. malayi* scRNA-seq dataset, Scanorama was used as an integration tool with publicly available *C. elegans* scRNA-seq datasets based on one-to-one orthologs (Hie et al., 2019). The pre-processed untreated *B. malayi* dataset was reduced to only genes that have a one-to-one ortholog in *C. elegans* followed by replacement of the *B. malayi* gene IDs to *C. elegans* gene IDs using Seurat. The Seurat object was then exported as an Ann Data object for input into Scanorama. The L2 larval stage specific dataset (Ben-David et al., 2020) and the most notable L4 larval stage dataset (CenGEN) (Taylor et al., 2021) were integrated with the subsetted *B. malayi* dataset with batch integration and plotted using ScanPy (Wolf et al., 2018).

Repetitive Pipettor (ReP)

The ReP is an automated, 3D-printed assembly that uses a DC motor (ServoCity, Winfield, KS), Raspberry Pi (rpi) Nano (CanaKit, North Vancouver, Canada), and an L298N motor controller (SunFounder, Shenzhen, China) to aspirate and dispense a p200 Eppendorf Research Plus pipette (Eppendorf, Hamburg, Germany) at any given rate, frequency, and volume. The structure was designed and modeled in Solidworks 2020 (https://www.solidworks.com/). The design includes six independent parts that were converted to STL files in Solidworks and sliced in Ultimaker Cura (https://github.com/Ultimaker/Cura) using the default printing settings of 0.2 mm layer height, 20% infill, and support material checked. The flat face of each part was positioned in contact with the build plate to reduce support material and refine rounded surfaces. Parts were printed using polylactic acid plastic filament and the support material was removed prior to assembly. Four pins were soldered to the rpi at pin locations 16, 18, 20, and 22. The rpi was subsequently glued to the 3D-printed structure at the four corner supports such that the SD card was facing upwards, and the USB and HDMI ports were facing outwards. The LN298 motor controller was glued to the opposite side of the structure such that the heat sink was facing downwards. For the rpi, ports 16, 18, and 22 were general purpose input/output pins and were connected to the IN1, IN2, and ENA ports of the motor controller, respectively. Port 20 was a ground inserted at the GND port of the motor controller. The 12-volt power supply had a positive and negative lead inserted into the motor controller at the +12V and GND ports, respectively. The OUT1 and OUT2 ports on the motor controller were finally wired and soldered to the motor terminals. All code was written in python, and the rpi was controlled remotely via SSH tunnels. All part files, protocol codes, and in-depth fabrication instructions can be found at https://github.com/emmakn/ReP.

Acknowledgements

The authors would like to thank the University of Wisconsin Carbone Cancer Center (UWCCC) Flow Lab and the Cancer Center Support Grant P30 CA014520 for assistance with flow cytometry. The UWCCCC Cytek Aurora Spectral Cytometer was made available through a NIH Shared Instrumentation Grant (Grant #: 1S10OD025225-01, Project Title: BD FACSymphony High Parameter Flow Cytometer). The authors would also like to thank the University of Wisconsin Biotechnology Center Gene Expression Center for facilitating single-cell and low-input RNA-sequencing. *Brugia* life cycle stages were obtained through the NIH/NIAID Filarial Research Reagent Resource Center (FR3), morphological voucher specimens are stored at the Harold W. Manter Museum at University of Nebraska, accession numbers P2021-2032. *C. elegans* strains were provided by the CGC, which is funded by NIH Office of Research Infrastructure Programs (P40 OD010440). Finally, the authors would like to thank Gabi Munoz for help optimizing single-cell suspensions and members of the Zamanian lab for constructive comments on the manuscript.

Funding

This work was supported by National Institutes of Health NIAID grant R01 AI151171 to MZ and the Wisconsin Alumni Research Foundation (WARF).

Competing Interests

The authors have declared no competing interests exist.

Supplemental Figure Legends

Supplementary Figure 1 - Optimization of SDS-DTT incubation by time and concentration
Supplementary Figure 2 - Mean gene and UMI counts of all clustered cells
Supplementary Figure 3 - UMAP visualization of marker genes used to annotate cell types
Supplementary Figure 4 - Distribution of neuronal transcripts across all cell clusters
Supplementary Figure 5 - Scanorama integration of *B. malayi* mf single-cell dataset and *C. elegans* L2 (Ben-David) and L4 (CeNGEN) datasets represented by library (A) and cell type (B)
Supplementary Figure 6 - Transcript abundance distribution across cell types for prominent antigens and zinc finger transcription factors (type C2H2)
Supplementary Figure 7 - Transcript abundance of anthelmintic targets across cell clusters

Supplementary File 1 - *B. malayi* differentially expressed genes from the FACS-sorted "largest" cell population
Supplementary File 2 - *C. elegans* differentially expressed genes from FACS-sorted large and GFP(+) cells
Supplementary File 3 - Gene expression comparison of untreated and IVM treated single-cell suspensions
Supplementary File 4 - Differentially expressed genes associated with secretory cells (cluster 15)
Supplementary File 5 - Comparison of cell counting methods by hemocytometer, flow cytometry, and automated cell counting instrument.

References

A. F. Bird JB. 1991. Secretory-Excretory System In: Bird AF, Bird J, editors. The Structure of Nematodes (Second Edition). San Diego: Academic Press, Inc. pp. 167–182. doi:10.1016/B978-0-12-099651-3.50015-0

Airs PM, Vaccaro K, Gallo KJ, Dinguirard N, Heimark ZW, Wheeler NJ, He J, Weiss KR, Schroeder NE, Huisken J, Zamanian M. 2022. Spatial transcriptomics reveals antiparasitic targets associated with essential behaviors in the human parasite Brugia malayi. *PLoS Pathog* **18**:e1010399. doi:10.1371/journal.ppat.1010399

Ballesteros C, Tritten L, O'Neill M, Burkman E, Zaky WI, Xia J, Moorhead A, Williams SA, Geary TG. 2016. The Effects of Ivermectin on Brugia malayi Females In Vitro: A Transcriptomic Approach. *PLoS Negl Trop Dis* **10**:e0004929. doi:10.1371/journal.pntd.0004929

Ben-David E, Boocock J, Guo L, Zdraljevic S, Bloom JS, Kruglyak L. 2020. Whole-organism mapping of the genetics of gene expression at cellular resolution. doi:10.1101/2020.08.23.263798

Bennuru S, Meng Z, Ribeiro JMC, Semnani RT, Ghedin E, Chan K, Lucas DA, Veenstra TD, Nutman TB. 2011. Stage-specific proteomic expression patterns of the human filarial parasite Brugia malayi and its endosymbiont Wolbachia. *Proc Natl Acad Sci U S A* **108**:9649–9654. doi:10.1073/pnas.1011481108

Campbell WC. 1982. Efficacy of the avermectins against filarial parasites: a short review. *Vet Res Commun* **5**:251–262.

Cao J, Packer JS, Ramani V, Cusanovich DA, Huynh C, Daza R, Qiu X, Lee C, Furlan SN, Steemers FJ, Adey A, Waterston RH, Trapnell C, Shendure J. 2017. Comprehensive single-cell transcriptional profiling of a multicellular organism. *Science* **357**:661–667. doi:10.1126/science.aam8940

Chippaux JP, Boussinesq M, Gardon J, Gardon-Wendel N, Ernould JC. 1996. Severe adverse reaction risks during mass treatment with ivermectin in loiasis-endemic areas. *Parasitol Today* **12**:448–450. doi:10.1016/0169-4758(96)40006-0

Chitwood and Chitwood. 1950. The Excretory SystemAn Introduction to Nematology. pp. 126–135.

Choi Y-J, Ghedin E, Berriman M, McQuillan J, Holroyd N, Mayhew GF, Christensen BM, Michalski ML. 2011. A deep sequencing approach to comparatively analyze the transcriptome of lifecycle stages of the filarial worm, Brugia malayi. *PLoS Negl Trop Dis* **5**:e1409. doi:10.1371/journal.pntd.0001409

Choudhary S, Abongwa M, Kashyap SS, Verma S, Mair GR, Kulke D, Martin RJ, Robertson AP. 2022. Nodulisporic acid produces direct activation and positive allosteric modulation of AVR-14B, a glutamate-gated chloride channel from adult Brugia malayi. *Proc Natl Acad Sci U S A* **119**:e2111932119. doi:10.1073/pnas.2111932119

Dent JA, Smith MM, Vassilatis DK, Avery L. 2000. The genetics of ivermectin resistance in Caenorhabditis elegans. *Proc Natl Acad Sci U S A* **97**:2674–2679. doi:10.1073/pnas.97.6.2674

Fuhrman JA, Piessens WF. 1985. Chitin synthesis and sheath morphogenesis in Brugia malayi microfilariae. *Mol Biochem Parasitol* **17**:93–104. doi:10.1016/0166-6851(85)90130-6

Galal M, Fujimaki Y, Shimada M, Aoki Y. 1989. Comparison of the Methods Available for Purification of Brugia pahangi Microfilariae in the Peritoneal Lavage of Jirds (Meriones unguiculatus). *Tropical Medicine* **31**:103–109.

Geary TG, Bourguinat C, Prichard RK. 2011. Evidence for macrocyclic lactone anthelmintic resistance in Dirofilaria immitis. *Top Companion Anim Med* **26**:186–192. doi:10.1053/j.tcam.2011.09.004

Geary TG, Woo K, McCarthy JS, Mackenzie CD, Horton J, Prichard RK, de Silva NR, Olliaro

PL, Lazdins-Helds JK, Engels DA, Bundy DA. 2010a. Unresolved issues in anthelmintic pharmacology for helminthiases of humans. *Int J Parasitol* **40**:1–13. doi:10.1016/j.ijpara.2009.11.001

Geary TG, Woo K, McCarthy JS, Mackenzie CD, Horton J, Prichard RK, de Silva NR, Olliaro PL, Lazdins-Helds JK, Engels DA, Bundy DA. 2010b. Unresolved issues in anthelmintic pharmacology for helminthiases of humans. *Int J Parasitol* **40**:1–13. doi:10.1016/j.ijpara.2009.11.001

Greene SE, Fischer K, Choi Y-J, Curtis KC, Budge PJ, Mitreva M, King CL, Fischer PU, Weil GJ. 2022. Characterization of a novel microfilarial antigen for diagnosis of Wuchereria bancrofti infections. *PLoS Negl Trop Dis* **16**:e0010407. doi:10.1371/journal.pntd.0010407

Hao Y, Hao S, Andersen-Nissen E, Mauck WM 3rd, Zheng S, Butler A, Lee MJ, Wilk AJ, Darby C, Zager M, Hoffman P, Stoeckius M, Papalexi E, Mimitou EP, Jain J, Srivastava A, Stuart T, Fleming LM, Yeung B, Rogers AJ, McElrath JM, Blish CA, Gottardo R, Smibert P, Satija R. 2021. Integrated analysis of multimodal single-cell data. *Cell* **184**:3573–3587.e29. doi:10.1016/j.cell.2021.04.048

Harischandra H, Yuan W, Loghry HJ, Zamanian M, Kimber MJ. 2018. Profiling extracellular vesicle release by the filarial nematode Brugia malayi reveals sex-specific differences in cargo and a sensitivity to ivermectin. *PLoS Negl Trop Dis* **12**:e0006438. doi:10.1371/journal.pntd.0006438

Harnett W. 2014. Secretory products of helminth parasites as immunomodulators. *Mol Biochem Parasitol* **195**:130–136. doi:10.1016/j.molbiopara.2014.03.007

Hewitson JP, Harcus YM, Curwen RS, Dowle AA, Atmadja AK, Ashton PD, Wilson A, Maizels RM. 2008. The secretome of the filarial parasite, Brugia malayi: proteomic profile of adult excretory-secretory products. *Mol Biochem Parasitol* **160**:8–21. doi:10.1016/j.molbiopara.2008.02.007

Hie B, Bryson B, Berger B. 2019. Efficient integration of heterogeneous single-cell transcriptomes using Scanorama. *Nat Biotechnol* **37**:685–691. doi:10.1038/s41587-019-0113-3

Higazi TB, Merriweather A, Shu L, Davis R, Unnasch TR. 2002. Brugia malayi: transient transfection by microinjection and particle bombardment. *Exp Parasitol* **100**:95–102. doi:10.1016/S0014-4894(02)00004-8

Higazi TB, Shu L, Unnasch TR. 2004. Development and transfection of short-term primary cell cultures from Brugia malayi. *Mol Biochem Parasitol* **137**:345–348. doi:10.1016/j.molbiopara.2004.06.004

Hotterbeekx A, Perneel J, Vieri MK, Colebunders R, Kumar-Singh S. 2021. The secretome of filarial nematodes and its role in host-parasite interactions and pathogenicity in onchocerciasis-associated epilepsy. *Front Cell Infect Microbiol* **11**:662766. doi:10.3389/fcimb.2021.662766

Ismail M, Botros S, Metwally A, William S, Farghally A, Tao LF, Day TA, Bennett JL. 1999. Resistance to praziquantel: direct evidence from Schistosoma mansoni isolated from Egyptian villagers. *Am J Trop Med Hyg* **60**:932–935. doi:10.4269/ajtmh.1999.60.932

Kaletsky R, Lakhina V, Arey R, Williams A, Landis J, Ashraf J, Murphy CT. 2016. The C. elegans adult neuronal IIS/FOXO transcriptome reveals adult phenotype regulators. *Nature* **529**:92–96. doi:10.1038/nature16483

Kalyanasundaram R, Khatri V, Chauhan N. 2020. Advances in Vaccine Development for Human Lymphatic Filariasis. *Trends Parasitol* **36**:195–205. doi:10.1016/j.pt.2019.11.005

Kang JS, Kim JS. 2000. Zinc finger proteins as designer transcription factors. *J Biol Chem* **275**:8742–8748. doi:10.1074/jbc.275.12.8742

Kashyap SS, Verma S, Voronin D, Lustigman S, Kulke D, Robertson AP, Martin RJ. 2019. Emodepside has sex-dependent immobilizing effects on adult Brugia malayi due to a differentially spliced binding pocket in the RCK1 region of the SLO-1 K channel. *PLoS*

Pathog **15**:e1008041. doi:10.1371/journal.ppat.1008041

Kaushal NA, Hussain R, Nash TE, Ottesen EA. 1982. Identification and characterization of excretory-secretory products of Brugia malayi, adult filarial parasites. *J Immunol* **129**:338–343.

Krause M, Harrison SW, Xu SQ, Chen L, Fire A. 1994. Elements regulating cell- and stage-specific expression of the C. elegans MyoD family homolog hlh-1. *Dev Biol* **166**:133–148. doi:10.1006/dbio.1994.1302

Krushna NSA, Shiny C, Dharanya S, Sindhu A, Aishwarya S, Narayanan RB. 2009. Immunolocalization and serum antibody responses to Brugia malayi pepsin inhibitor homolog (Bm-33). *Microbiol Immunol* **53**:173–183. doi:10.1111/j.1348-0421.2009.00114.x

Lalitha P, Eswaran D, Gnanasekar M, Rao KVN, Narayanan RB, Scott A, Nutman T, Kaliraj P. 2002. Development of antigen detection ELISA for the diagnosis of brugian and bancroftian filariasis using antibodies to recombinant filarial antigens Bm-SXP-1 and Wb-SXP-1. *Microbiol Immunol* **46**:327–332. doi:10.1111/j.1348-0421.2002.tb02703.x

Lamassiaude N, Courtot E, Corset A, Charvet CL, Neveu C. 2022. Pharmacological characterization of novel heteromeric GluCl subtypes from Caenorhabditis elegans and parasitic nematodes. *Br J Pharmacol* **179**:1264–1279. doi:10.1111/bph.15703

Landmann F, Foster JM, Slatko B, Sullivan W. 2010. Asymmetric Wolbachia segregation during early Brugia malayi embryogenesis determines its distribution in adult host tissues. *PLoS Negl Trop Dis* **4**:e758. doi:10.1371/journal.pntd.0000758

Li BW, Rush AC, Weil GJ. 2014. High level expression of a glutamate-gated chloride channel gene in reproductive tissues of Brugia malayi may explain the sterilizing effect of ivermectin on filarial worms. *Int J Parasitol Drugs Drug Resist* **4**:71–76. doi:10.1016/j.ijpddr.2014.01.002

Lightowlers MW, Rickard MD. 1988. Excretory-secretory products of helminth parasites: effects on host immune responses. *Parasitology* **96 Suppl**:S123–66. doi:10.1017/s0031182000086017

Liu C, Grote A, Ghedin E, Unnasch TR. 2020. CRISPR-mediated Transfection of Brugia malayi. *PLoS Negl Trop Dis* **14**:e0008627. doi:10.1371/journal.pntd.0008627

Liu C, Mhashilkar AS, Chabanon J, Xu S, Lustigman S, Adams JH, Unnasch TR. 2018. Development of a toolkit for piggyBac-mediated integrative transfection of the human filarial parasite Brugia malayi. *PLoS Negl Trop Dis* **12**:e0006509. doi:10.1371/journal.pntd.0006509

Local Burden of Disease 2019 Neglected Tropical Diseases Collaborators. 2020. The global distribution of lymphatic filariasis, 2000-18: a geospatial analysis. *Lancet Glob Health* **8**:e1186–e1194. doi:10.1016/S2214-109X(20)30286-2

Loghry HJ, Yuan W, Zamanian M, Wheeler NJ, Day TA, Kimber MJ. 2020. Ivermectin inhibits extracellular vesicle secretion from parasitic nematodes. *J Extracell Vesicles* **10**:e12036. doi:10.1002/jev2.12036

Maizels RM, Gomez-Escobar N, Gregory WF, Murray J, Zang X. 2001. Immune evasion genes from filarial nematodes. *Int J Parasitol* **31**:889–898. doi:10.1016/s0020-7519(01)00213-2

Mattingly BC, Buechner M. 2011. The FGD homologue EXC-5 regulates apical trafficking in C. elegans tubules. *Dev Biol* **359**:59–72. doi:10.1016/j.ydbio.2011.08.011

McInnes L, Healy J, Saul N, Großberger L. 2018. UMAP: Uniform Manifold Approximation and Projection. *J Open Source Softw* **3**:861. doi:10.21105/joss.00861

McLaren DJ. 1972. Ultrastructural studies on microfilariae (Nematoda: Filarioidea). *Parasitology* **65**:317–332. doi:10.1017/s0031182000045108

Michalski ML, Griffiths KG, Williams SA, Kaplan RM, Moorhead AR. 2011. The NIH-NIAID Filariasis Research Reagent Resource Center. *PLoS Negl Trop Dis* **5**:e1261. doi:10.1371/journal.pntd.0001261

Moreno Y, Geary TG. 2008. Stage- and gender-specific proteomic analysis of Brugia malayi excretory-secretory products. *PLoS Negl Trop Dis* **2**:e326. doi:10.1371/journal.pntd.0000326

Moreno Y, Geary TG, Tritten L. 2021. When Secretomes Meet Anthelmintics: Lessons for Therapeutic Interventions. *Trends Parasitol* **37**:468–475. doi:10.1016/j.pt.2021.01.007

Moreno Y, Nabhan JF, Solomon J, Mackenzie CD, Geary TG. 2010. Ivermectin disrupts the function of the excretory-secretory apparatus in microfilariae of Brugia malayi. *Proc Natl Acad Sci U S A* **107**:20120–20125. doi:10.1073/pnas.1011983107

Morris CP, Bennuru S, Kropp LE, Zweben JA, Meng Z, Taylor RT, Chan K, Veenstra TD, Nutman TB, Mitre E. 2015. A Proteomic Analysis of the Body Wall, Digestive Tract, and Reproductive Tract of Brugia malayi. *PLoS Negl Trop Dis* **9**:e0004054. doi:10.1371/journal.pntd.0004054

Morris CP, Evans H, Larsen SE, Mitre E. 2013. A comprehensive, model-based review of vaccine and repeat infection trials for filariasis. *Clin Microbiol Rev* **26**:381–421. doi:10.1128/CMR.00002-13

Mutafchiev Y, Bain O, Williams Z, McCall JW, Michalski ML. 2014. Intraperitoneal development of the filarial nematode Brugia malayi in the Mongolian jird (Meriones unguiculatus). *Parasitol Res* **113**:1827–1835. doi:10.1007/s00436-014-3829-5

Nelson FK, Riddle DL. 1984. Functional study of the Caenorhabditis elegans secretory-excretory system using laser microsurgery. *J Exp Zool* **231**:45–56. doi:10.1002/jez.1402310107

Ni Z, Chen S, Brown J, Kendziorski C. 2020. CB2 improves power of cell detection in droplet-based single-cell RNA sequencing data. *Genome Biol* **21**:137. doi:10.1186/s13059-020-02054-8

Osei-Atweneboana MY, Awadzi K, Attah SK, Boakye DA, Gyapong JO, Prichard RK. 2011. Phenotypic evidence of emerging ivermectin resistance in Onchocerca volvulus. *PLoS Negl Trop Dis* **5**:e998. doi:10.1371/journal.pntd.0000998

Packer JS, Zhu Q, Huynh C, Sivaramakrishnan P, Preston E, Dueck H, Stefanik D, Tan K, Trapnell C, Kim J, Waterston RH, Murray JI. 2019. A lineage-resolved molecular atlas of C. elegans embryogenesis at single-cell resolution. *Science* **365**. doi:10.1126/science.aax1971

Park S-K, Gunaratne GS, Chulkov EG, Moehring F, McCusker P, Dosa PI, Chan JD, Stucky CL, Marchant JS. 2019. The anthelmintic drug praziquantel activates a schistosome transient receptor potential channel. *J Biol Chem* **294**:18873–18880. doi:10.1074/jbc.AC119.011093

Peter N. Inglis, Guangshuo Ou, Michel R. Leroux, and Jonathan M. Scholey. 2006. The sensory cilia of Caenorhabditis elegans In: The C. elegans Research Community, editor. WormBook. WormBook ed. doi:doi/10.1895/wormbook.1.126.1

Philogene MC, Small SGM, Wang P, Corsi AK. 2012. Distinct Caenorhabditis elegans HLH-8/twist-containing dimers function in the mesoderm. *Dev Dyn* **241**:481–492. doi:10.1002/dvdy.23734

Qing X, Kulkeaw K, Wongkamchai S, Tsui SK-W. 2021. Mitochondrial Genome of Brugia malayi Microfilariae Isolated From a Clinical Sample. *Frontiers in Ecology and Evolution* **9**:25. doi:10.3389/fevo.2021.637805

Rao UR, Chandrashekar R, Subrahmanyam D. 1987. Effect of ivermectin on serum dependent cellular interactions to Dipetalonema viteae microfilariae. *Trop Med Parasitol* **38**:123–127.

Rathaur S, Robertson BD, Selkirk ME, Maizels RM. 1987. Secretory acetylcholinesterases from Brugia malayi adult and microfilarial parasites. *Mol Biochem Parasitol* **26**:257–265. doi:10.1016/0166-6851(87)90078-8

Razin SV, Borunova VV, Maksimenko OG, Kantidze OL. 2012. Cys2His2 zinc finger protein family: classification, functions, and major members. *Biochemistry* **77**:217–226. doi:10.1134/S0006297912030017

Reaves BJ, Wallis C, McCoy CJ, Lorenz WW, Rada B, Wolstenholme AJ. 2018. Recognition and killing of Brugia malayi microfilariae by human immune cells is dependent on the parasite sample and is not altered by ivermectin treatment. *Int J Parasitol Drugs Drug Resist* **8**:587–595. doi:10.1016/j.ijpddr.2018.09.002

Roberts L, Schmidt GD, Janovy J Jr. 2009. Foundations of Parasitology. McGraw-Hill Education.

Sundaram MV, Buechner M. 2016. The Caenorhabditis elegans Excretory System: A Model for Tubulogenesis, Cell Fate Specification, and Plasticity. *Genetics* **203**:35–63. doi:10.1534/genetics.116.189357

Taylor SR, Santpere G, Weinreb A, Barrett A, Reilly MB, Xu C, Varol E, Oikonomou P, Glenwinkel L, McWhirter R, Poff A, Basavaraju M, Rafi I, Yemini E, Cook SJ, Abrams A, Vidal B, Cros C, Tavazoie S, Sestan N, Hammarlund M, Hobert O, Miller DM. 2020. Molecular topography of an entire nervous system. *Cell*. doi:10.1016/j.cell.2021.06.023

Tongu Y. 1974. Ultrastructural studies on the microfilaria of Brugia malayi. *Acta Med Okayama* **28**:219–242.

Ton TGN, Mackenzie C, Molyneux DH. 2015. The burden of mental health in lymphatic filariasis. *Infect Dis Poverty* **4**:34. doi:10.1186/s40249-015-0068-7

U. R. Rao, A. C. Vickery, B. H. Kwa, J. K. Nayar. 1992. Brugia Malayi: Ivermectin Inhibits the Exsheathment of Microfilariae. *ASTMH* **46**:183–188. doi:10.4269/ajtmh.1992.46.183

Vatta AF, Dzimianski M, Storey BE, Camus MS, Moorhead AR, Kaplan RM, Wolstenholme AJ. 2014. Ivermectin-dependent attachment of neutrophils and peripheral blood mononuclear cells to Dirofilaria immitis microfilariae in vitro. *Vet Parasitol* **206**:38–42. doi:10.1016/j.vetpar.2014.02.004

Verma S, Kashyap SS, Robertson AP, Martin RJ. 2020. Diethylcarbamazine activates TRP channels including TRP-2 in filaria, Brugia malayi. *Communications Biology* **3**:398. doi:10.1038/s42003-020-01128-4

Weiss MG. 2008. Stigma and the social burden of neglected tropical diseases. *PLoS Negl Trop Dis* **2**:e237. doi:10.1371/journal.pntd.0000237

Williams PDE, Kashyap SS, McHugh MA, Robertson AP, Martin RJ. 2022. Diethylcarbamazine, TRP channels and Ca2+ signaling in cells of the Ascaris intestine. *Research Square*. doi:10.21203/rs.3.rs-1262219/v1

Wolf FA, Angerer P, Theis FJ. 2018. SCANPY: large-scale single-cell gene expression data analysis. *Genome Biol* **19**:15. doi:10.1186/s13059-017-1382-0

Wolstenholme AJ, Evans CC, Jimenez PD, Moorhead AR. 2015. The emergence of macrocyclic lactone resistance in the canine heartworm, Dirofilaria immitis. *Parasitology* **142**:1249–1259. doi:10.1017/S003118201500061X

World Health Organization. 2018. Guideline: Alternative Mass Drug Administration Regimens to Eliminate Lymphatic Filariasis. Geneva: World Health Organization.

Wu Y, Preston G, Bianco AE. 2008. Chitinase is stored and secreted from the inner body of microfilariae and has a role in exsheathment in the parasitic nematode Brugia malayi. *Mol Biochem Parasitol* **161**:55–62. doi:10.1016/j.molbiopara.2008.06.007

Xu S, Liu C, Tzertzinis G, Ghedin E, Evans CC, Kaplan R, Unnasch TR. 2011. In vivo transfection of developmentally competent Brugia malayi infective larvae. *Int J Parasitol* **41**:355–362. doi:10.1016/j.ijpara.2010.10.005

Young MD, Behjati S. 2020. SoupX removes ambient RNA contamination from droplet-based single-cell RNA sequencing data. *Gigascience* **9**. doi:10.1093/gigascience/giaa151

Zahner H, Schmidtchen D, Mutasa JA. 1997. Ivermectin-induced killing of microfilariae in vitro by neutrophils mediated by NO. *Exp Parasitol* **86**:110–117. doi:10.1006/expr.1997.4160

Zamanian M, Fraser LM, Agbedanu PN, Harischandra H, Moorhead AR, Day TA, Bartholomay LC, Kimber MJ. 2015. Release of Small RNA-containing Exosome-like Vesicles from the Human Filarial Parasite Brugia malayi. *PLoS Negl Trop Dis* **9**:e0004069.

doi:10.1371/journal.pntd.0004069

Zhang S, Banerjee D, Kuhn JR. 2011. Isolation and culture of larval cells from C. elegans. *PLoS One* **6**:e19505. doi:10.1371/journal.pone.0019505